Ancient TL

A periodical devoted to Luminescence and ESR dating

Volume 29 No.1   June 2011

Ancient TL

Started by the late David Zimmerman in 1977

Ancient TL

A periodical devoted to Luminescence and ESR dating

Web site: http://www.aber.ac.uk/ancient-tl

What date is it? Should there be an agreed datum for luminescence ages?

G.A.T. Duller

Institute of Geography and Earth Sciences, Aberystwyth University, Aberystwyth, Ceredigion SY23 3DB, United Kingdom (email: ggd@aber.ac.uk)

_____

Introduction

Wolfe (2007) recently highlighted the lack of an agreed common datum for most Quaternary chronological methods, and this was a topic also taken up by Grün (2008). The problem is that for many chronological methods, the value that is determined is the number of years that have passed between the event that is being dated and when the sample was collected, or when it was measured. Under such a system, an event in the past inevitably becomes further distant in time as time progresses. The eruption of Mt Pinatubo in the Philippines occurred in AD 1991, which today (AD 2011) means that it occurred 20 years ago. In the year AD2020 the event would have an age of 29 years ago.

At present only radiocarbon dating has an agreed system for quoting ages that is not affected by this. As agreed by the International Radiocarbon Conference all ages are quoted as ^{14}C years BP (before present), where the present is defined as AD 1950 (van der Plicht and Hogg 2006). The situation in radiocarbon dating is made more complex by the need to calibrate ages to overcome the effects of changes in the production of radiocarbon and its distribution between the different carbon reservoirs. However, this does not alter the situation that this method alone has defined a datum for its results, avoiding ambiguity when quoting ages.

Quaternary dating methods which do not have an agreed datum, including luminescence, normally solve the problem in one of two ways. The most common is that when ages are published, the year of measurement is quoted, and ages are given relative to that year. For instance Bristow et al. (2007) quoted ages (e.g. 34 ± 7 a) for recent samples from linear dunes in the Namib Sand Sea relative to AD 2004 when the ages were calculated. The second approach is to convert ages as given above to the Christian calendar and use AD (anno domini) and BC (before Christ). Thus the age of 34 ± 7 a measured in AD 2004 given above would equate to a date of AD1970 ± 7 a or AD1963 - 1977.

However, all of these alternatives have problems. Quoting ages relative to an age quoted in a table is scientifically accurate and leaves no uncertainty, but two issues arise. The first is that if the same event were dated at some different time, say 20 years earlier (in AD 1984) or 20 years later (in AD 2024) then different ages would be obtained (14 ± 7 a and 54 ± 7 a), yet in fact all these different age estimates are giving exactly the same estimate of when this event occurred. This is confusing, but not incorrect. The second issue can also be illustrated with this example. If at some stage all the ages for this event are collated then there is a risk that the person undertaking the summary will fail to take into account the different dates used for the datum of each analysis, or that in their summary table the year in which the ages were measured will not be included. The recent compilation of ages in the Namib Sand Sea digital database is such an example where ages have been compiled (Livingstone et al., 2010).

Quoting ages using AD or BC avoids this problem by using the datum of 1 BC / 1 AD. This solution enables ages to be quoted accurately and with no ambiguity. However, two potential difficulties arise here. The first is a simple numerical one. The construction of the timescale using AD and BC means that the numerical value arising increases both since the datum of 1 AD and prior to the datum. Thus one has both AD 100 and BC 100 (positive numerical values) even though one event is prior to the datum and one postdates it. The second is that geomorphologists and Quaternary scientists do not tend to work in AD and BC.

Luminescence is not unique among Quaternary geochronological methods in facing this problem. However, because of the age range now covered by luminescence, from hundreds of thousands of years to decades or even years (e.g. Madsen and Murray, 2009; Rink and Lopez, 2010; Rustomji and Pietsch, 2007; Wolf and Hugenholtz, 2009), the luminescence community is uniquely affected by the issue.

Additionally, with the growth of luminescence in recent decades, it is probably the second most widely used Quaternary radiometric method after radiocarbon.

Alternatives

I suggest that we have a number of alternatives when facing this issue:

1) The status quo.

Retain the practise of quoting luminescence ages along with the year in which they were measured, and thus leaving users to convert these into years AD or BC, or to compensate for differences between ages obtained in different years.

2) Adopt a datum of AD 1950 and use the term BP.

The use of the term BP (before present) has historically been specifically reserved for use with radiocarbon dates. Radiocarbon dates are often quoted in radiocarbon years before present (^{14}C yrs BP) and since the Libby half-life is used for such calculations, ^{14}C years are not equivalent to calendar years. Luminescence dates are calculated in calendar years and so adopting this term for luminescence would cause confusion.

3) Adopt a datum of AD 1950 and use an alternative term instead of BP.

Given the widespread use of 1950 as a datum by radiocarbon, this would provide a useful point of comparison. Once radiocarbon ages are calibrated into calendar years then ages from both methods should be directly comparable. An alternative term to BP would be required (for the reasons stated above).

4) Adopt a datum of AD 2000 and use the term b2k.

An alternative datum would be the year AD 2000. The use of a different datum and a different term (b2k instead of BP) would help to avoid confusion between uncalibrated radiocarbon dates and those from other methods which are not affected by the same issues of calibration due to changes in the production of radiocarbon. The term b2k (before 2000 AD) is one which is now being used increasingly by other dating methods (e.g. Walker et al., 2009).

I would strongly suggest that option 2 is not appropriate. The term BP has a very specific scientific meaning that is relevant to radiocarbon dating, but cannot be transferred to other methods. I would also suggest that option 3 would lead to confusion. One implication of adopting either option 3 or 4 above is that we will rapidly start to produce ages that are quoted as negative ages. For instance, if we were to adopt AD 2000 as the datum then an age

of 7±2 a produced in AD 2010 would be presented as -3 ± 2 a b2k. At first sight this appears awkward since we are dating an event which is in the past, but it is quoted as a negative age because the event occurred after our datum. Such a situation is inevitable if we choose to adopt a datum.

What should happen next?

This is a decision that needs to be discussed by as wide a community as possible, and then an agreed decision made. A good venue for such an agreement would be at the International Luminescence and Electron Spin Resonance dating conference which is held once every three years. The next conference will be in Poland in July 2011, and I would suggest that this issue be discussed in open forum at that time for the community to come to a decision upon, and potentially to vote upon if the community felt that this was appropriate. For those colleagues who are unable to attend the meeting in Poland I would ask them to write to me, or to ask colleagues to present their views at that meeting.

Once a decision has been made then it should be disseminated as widely as possible amongst the luminescence community and the wider geomorphological, Quaternary and archaeological communities to ensure that it is used as widely as possible. This could be done through the special issues associated with the LED 2011 conference, and by writing to editors of key journals in the field.

References

Grün, R. (2008) Special Issue – Prospects for the new frontiers of earth and environmental sciences. *Quaternary Geochronology* **3**, 173.

Livingstone, I., Bristow, C. S., Bryant, R. G., Bullard, J., White, K., Wiggs, G. F. S., Baas, A. C. W., Bateman, M. D., Thomas, D. S. G. (2010). The Namib Sand Sea digital database of aeolian dunes and key forcing variables. *Aeolian Research* **2**, 93-104.

Madsen, A. T., Murray, A. S. (2009). Optically stimulated luminescence dating of young sediments: A review. *Geomorphology* **109**, 3-16.

Rink, W. J., Lopez, G. I. (2010). OSL-based lateral progradation and aeolian sediment accumulation rates for the Apalachicola Barrier Island Complex, North Gulf of

Mexico, Florida. *Geomorphology* **123**, 330-342.

Rose, J. (2007). The use of time units in Quaternary Science Reviews. *Quaternary Science Reviews* **26**, 1193.

Rustomji, P. and Pietsch, T. (2007). Alluvial sedimentation rates from southeastern Australia indicate post-European settlement landscape recovery. *Geomorphology* **90**, 73-90.

van der Plicht, J., Hogg, A. (2006). A note on reporting radiocarbon. *Quaternary Geochronology* **1**, 237-240.

Walker, M., Johnsen, S., Rasmussen, S. O., Popp, T., Steffensen, J. P., Gibbard, P., Hoek, W., Lowe, J., Andrews, J., Bjorck, S., Cwynar, L. C., Hughen, K., Kershaw, P., Kromer, B., Litt, T., Lowe, D. J., Nakagawa, T., Newnham, R., Schwander, J. (2009). Formal definition and dating of the GSSP (Global Stratotype Section and Point) for the base of the Holocene using the Greenland NGRIP ice core, and selected auxiliary records. *Journal of Quaternary Science* **24**, 3-17.

Wolfe, S. A., Hugenholtz, C. H. (2009). Barchan dunes stabilized under recent climate warming on the northern Great Plains. *Geology* **37**, 1039-1042.

Wolff, E. W. (2007). When is the present? *Quaternary Science Reviews* **26**, 3023-3024.

Reviewer
R. Grün

Dose-rate conversion factors: update

G. Guérin[1,*], N. Mercier[1], G. Adamiec[2]

[1]Institut de Recherche sur les Archéomatériaux, UMR 5060 CNRS - Université de Bordeaux, Centre de Recherche en Physique Appliquée à l'Archéologie (CRP2A), Maison de l'archéologie, 33607 Pessac cedex, France
[2]Department of Radioisotopes, Institute of Physics, Silesian University of Technology, ul. Krzywoustego 2, 44-100 Gliwice, Poland
[*] Corresponding Author : guillaumeguerin@ymail.com (G. Guérin)

Abstract
In the field of luminescence and electron spin resonance dating, dose rate conversion factors are widely used to convert concentrations of radioactive isotopes to dose rate values. These factors are derived from data provided by the National Nuclear Data Center of the Brookhaven National Laboratory, which are compiled in Evaluated Nuclear Structure Data Files (ENSDF) and Nuclear Wallet Cards. The recalculated dose rate conversion factors are a few percent higher than those previously published, except for beta and gamma emissions of the isotopes of the U-series decay chains.

Introduction
In luminescence and electron spin resonance dating, an age is obtained by dividing the palaeodose with the dose-rate that an object to be dated has been exposed to. The latter is determined by measurements of concentrations of radioelements or activity using gamma spectrometry, ICP MS, neutron activation analysis, alpha counting, beta counting or flame photospectrometry. The elemental concentrations are then converted in dose rates using conversion factors. These depend on the properties of the nuclear decays involved. The conversion factors have been calculated from time to time, for example by Nambi and Aitken (1986) or Adamiec and Aitken (1998; see also references therein) based on the ENSDF data. However, a new data set is available and an update is timely. The data used here were downloaded on 5th November 2009 on the Chart of Nuclides (http://www.nndc.bnl.gov/chart/index.jsp) and are based on Evaluated Nuclear Structure Data Files (ENSDF) and Nuclear Wallet Cards. This paper presents updated conversion factors following the approach of Adamiec and Aitken (1998).

The data
Tables 1 and 2 show the energy emission values for the ^{232}Th, ^{238}U and ^{235}U and series for alpha, beta and gamma rays as derived from the data of the National Brookhaven Laboratory website. The most appreciable differences between the data in these tables and those of Adamiec and Aitken (1998) are in the ^{235}U series, since updated values for these radioelements have been published since 1998 (e.g. Browne, 2001) for ^{231}Th, ^{231}Pa, ^{227}Ac, ^{227}Th, ^{223}Fr, ^{223}Ra, ^{219}Rn.

The dose-rate values are given for infinite matrices (Aitken, 1985), for secular equilibrium of the radioactive decay chains as well as for total radon escape. Table 2 presents dose rate data for natural uranium, taking account of isotopic abundances (mass fractions: 99.29% for ^{238}U and 0.71% for ^{235}U). It should be noted here that the infinite matrix assumption implies homogeneity in absorption coefficients; taking account of different absorption characteristics between e.g. X-rays and gamma rays would require Monte Carlo modelling and is therefore beyond the scope of this paper.

Data for potassium and rubidium are given in Table 3. It should be noted that there is a significant difference for the potassium because the half-life of ^{40}K was recently reevaluated (Grau Malonda & Grau Carles, 2002; Kossert & Gunther, 2004) and is now 2.3% lower than previously published.

Concluding remarks
Even though uncertainty factors such as moisture content, heterogeneity of sedimentary media etc. have significant effects on the accuracy of dose rate , it is of paramount importance to minimize all sources of systematic errors. The overall effect of our update obviously depends on each case, but may reach a few percent on the final obtained age calculation. We therefore recommend that our newest conversion factors, which are derived from the up-to-date nuclear data, should be henceforth used for luminescence and ESR age calculations.

Table 1: *Energy release and dose rates in the ^{232}Th decay series.*

Isotope	Half-life (s)	Alpha		Beta		Gamma	
		Energy	Dose rate	Energy	Dose rate	Energy	Dose rate
^{232}Th	4.43 10^{17}	4.003	0.0821	0.0113	0.0002	0.0011	0.0000
^{228}Ra	1.81 10^{8}	-	-	0.0092	0.0002	0.0004	0.0000
^{228}Ac	2.21 10^{4}	-	-	0.4171	0.0086	0.8602	0.0176
^{228}Th	6.03 10^{7}	5.406	0.1109	0.0195	0.0004	0.0031	0.0001
^{224}Ra	3.16 10^{5}	5.673	0.1164	0.0023	0.0000	0.0104	0.0002
^{220}Rn	5.56 10^{1}	6.288	0.1290	-	-	0.0006	0.0000
^{216}Po	1.45 10^{-1}	6.778	0.1390	-	-	0.0000	0.0000
^{212}Pb	3.83 10^{4}	-	-	0.1721	0.0035	0.1437	0.0029
^{212}Bi	3.63 10^{3}	2.175	0.0446	0.5034	0.0103	0.1039	0.0021
^{212}Po (0.641)	2.99 10^{-4}	5.631	0.1155	-	-	-	-
^{208}Tl (0.359)	1.83 10^{2}	-	-	0.2140	0.0044	1.2136	0.0249
Total		**0.7375**		**0.0277**		**0.0479**	
Pre-Rn total		**0.3093**		**0.0094**		**0.0180**	
Adamiec & Aitken (1998)							
Total		0.7320		0.0273		0.0476	
Pre-Rn total		0.3050		0.0091		0.0178	
Rel. Difference (%)							
Total		0.75%		1.34%		0.70%	
Pre-Rn total		1.42%		3.53%		0.84%	

Notes for table 1.

1. Energies are given in MeV and represent the energy emitted per disintegration.
2. Branching ratios are shown in parenthesis against the radioelements in the branches; associated values given for energy release are after adjustment for branching. Note that the branching also affects the energy release of the radioelement at which the branching occurs; thus the value given for the alpha release by ^{212}Bi is 35.9% of the full energy - because ^{208}Tl is formed by alpha emission from ^{212}Bi.
3. Beta components include Auger electrons and internal conversion; gamma components include X-rays and annihilation radiation; alpha recoil and neutrinos are not included due to their insignificant contribution to dose-rates (cf. Adamiec and Aitken, 1998).
5. A dash indicates that no radiation of that type is mentioned by the National Nuclear Data Centre.
6. Dose rate values are given in Gy ka^{-1} per ppm of parent (i.e. mg of parent per kg of sample), assuming equilibrium in the decay chains. The activity of the parent is 4.057 Bq kg^{-1} of sample.
7. The rows labelled 'pre-Rn' give the values for 100% escape of radon.
8. Relative differences are calculated between this paper and values from Adamiec and Aitken (1998).
9. ^{216}At has been omitted since its contribution to the total energy is insignificant.

Table 2: *Energy release and dose rates in the uranium (^{238}U and ^{235}U) decay series.*

Isotope	Half-life (s)	Alpha			Beta			Gamma		
		Energy	Dose rate	Dose rate, nat. U	Energy	Dose rate	Dose rate, nat. U	Energy	Dose rate	Dose rate, nat. U
^{238}U	1.41 10^{17}	4.193	0.264	0.262	0.007	0.0005	0.0004	0.001	0.0001	0.0001
^{234}Th	2.08 10^{6}	-	-	-	0.059	0.0037	0.0037	0.008	0.0005	0.0005
^{234}Pa$_m$	6.95 10^{1}	-	-	-	0.810	0.0509	0.0506	0.016	0.0010	0.0010
^{234}Pa $_{(0.0016)}$	2.41 10^{4}	-	-	-	0.001	0.0001	0.0001	0.001	0.0001	0.0001
^{234}U	7.75 10^{12}	4.759	0.299	0.297	0.012	0.0007	0.0007	0.001	0.0001	0.0001
^{230}Th	2.38 10^{12}	4.664	0.293	0.291	0.013	0.0008	0.0008	0.001	0.0001	0.0001
^{226}Ra	5.05 10^{10}	4.775	0.300	0.298	0.004	0.0002	0.0002	0.007	0.0005	0.0005
^{222}Rn	3.30 10^{5}	5.489	0.345	0.343	-	-	-	0.000	0.0000	0.0000
^{218}Po	1.86 10^{2}	6.001	0.377	0.375	-	-	-	-	-	-
^{214}Pb	1.61 10^{3}	-	-	-	0.291	0.0183	0.0182	0.239	0.0150	0.0149
^{214}Bi	1.19 10^{3}	0.001	0.000	0.000	0.654	0.0411	0.0408	1.475	0.0928	0.0921
^{214}Po	1.64 10^{-4}	7.687	0.483	0.480	-	-	-	0.000	0.0000	0.0000
^{210}Pb	7.01 10^{8}	-	-	-	0.033	0.0021	0.0021	0.005	0.0003	0.0003
^{210}Bi	4.33 10^{5}	-	-	-	0.389	0.0245	0.0243	-	-	-
^{210}Po	1.20 10^{7}	5.304	0.333	0.331	0.000	0.0000	0.0000	0.000	0.0000	0.0000
^{238}U total			2.695	2.676		0.1429	0.1419		0.1104	0.1096
^{238}U Pre-Rn total			1.156	1.148		0.0570	0.0566		0.0022	0.0022
^{235}U	2.22 10^{16}	4.114	1.663	0.012	0.029	0.0117	0.0001	0.164	0.0665	0.0005
^{231}Th	2.20 10^{6}	-	-	-	0.146	0.0591	0.0004	0.023	0.0094	0.0001
^{231}Pa	1.03 10^{12}	4.924	1.990	0.014	0.032	0.0130	0.0001	0.040	0.0160	0.0001
^{227}Ac	6.87 10^{8}	0.070	0.028	0.000	0.012	0.0049	0.0000	0.001	0.0002	0.0000
^{227}Th $_{(0.986)}$	1.61 10^{6}	5.808	2.347	0.017	0.050	0.0202	0.0001	0.154	0.0621	0.0004
^{223}Fr $_{(0.014)}$	1.32 10^{3}	0.005	0.002	0.000	0.000	0.0002	0.0000	0.001	0.0003	0.0000
^{223}Ra	9.88 10^{5}	5.664	2.289	0.016	0.068	0.0275	0.0002	0.135	0.0546	0.0004
^{219}Rn	3.96 10^{0}	6.753	2.729	0.019	0.007	0.0027	0.0000	0.058	0.0235	0.0002
^{215}Po	1.78 10^{-3}	7.392	2.987	0.021	-	-	-	-		
^{211}Pb	2.17 10^{3}	-	-	-	0.450	0.1817	0.0013	0.064	0.0258	0.0002
^{211}Bi	1.28 10^{2}	6.549	2.647	0.019	0.013	0.0053	0.0000	0.047	0.0191	0.0001
^{211}Po	5.16 10^{-1}	0.021	0.008	0.000	-	-	-	-	-	-
^{207}Tl	2.86 10^{2}	-	-	-	0.495	0.2002	0.0014	0.002	0.0009	0.0000
^{235}U total			16.690	0.1185		0.5265	0.0037		0.2807	0.0020
Total			**2.795**			**0.1457**			**0.1116**	
Pre-Rn total			**1.267**			**0.0603**			**0.0042**	
Adamiec & Aitken (1998)										
Total			2.78			0.146			0.113	
Pre-Rn total			1.26			0.06			0.0044	
Rel. Difference (%)										
Total			0.53%			-0.24%			-1.28%	
Pre-Rn total			0.52%			0.54%			-4.43%	

Notes for table 2.

1. See notes 1-8 of Table 1.

2. The mass abundances used in the natural uranium calculations for ^{238}U and ^{235}U (respectively 99.29% and 0.71%) correspond to the natural atomic abundances of 99.28% and 0.72% respectively.

3. The activity of the parent (per ppm of parent) is 12.44 Bq kg^{-1} of sample for ^{238}U, 79.94 for ^{235}U and 12.92 for natural uranium.

4. The rows labelled 'pre-Rn' give the values for 100% escape of radon in the case of ^{238}U series, but because of the short half-life of ^{219}Rn the values given for natural uranium include contributions of that gas and its daughters.

5. ^{218}At, ^{218}Rn, ^{210}Tl, ^{206}Tl and ^{215}At have been omitted since their contribution to the total is insignificant.

Table 3: *Dose-rate data for Potassium and Rubidium.*

		[40]K	[87]Rb
Natural abundance (mg.g^{-1})		0.119	283
Half-life (Ga)		1.248	48.1
Average energy per disintegration (MeV)	Beta	0.499	0.0817
	Gamma	0.1557	
Specific activity (Bq.kg^{-1}) for concentration of 1% nat. K and 50 ppm of nat. Rb	Total	316.4	44.8
	Beta	282.5	44.8
	Gamma	33.73	
Dose-rate (Gy.ka[-1]) for concentrations as above	Beta	0.7982	0.0185
	Gamma	0.2491	
Dose-rate, Adamiec & Aitken (1998)	Beta	0.782	0.019
	Gamma	0.243	
Relative differences	Beta	2.07%	-2.67%
	Gamma	2.49%	

Notes for table 3.
1. The energy given for potassium is that released per disintegration, i.e. after allowance for branching between beta and gamma (89.28% and 10.72% respectively).
2. The contents given in row 1 correspond to natural atomic abundances of 116.7 ppm and 27.8%.

References
Adamiec, G., Aitken, M.J. (1998). Dose-rate conversion factors: update. *Ancient TL* **16**, 37-50.
Aitken, M.J. (1985). *Thermoluminescence dating*. Academic Press, London.
Browne, E. (2001). Nuclear Data Sheets for A = 215,219,223,227,231. *Nuclear Data Sheets* **93**, 763-1061.
Grau Malonda, A., Grau Carles, A. (2002). Half-life determination of [40]K by LSC Measurements. *Applied Radiation and Isotopes* **56**, 153-156.
Kossert, K., Gunther, E. (2004). LSC Measurements of Half-life of [40]K. *Applied Radiation and Isotopes* **60**, 459-464.
Nambi, K.S.V., Aitken, M.J. (1986). Annual dose conversion factors for TL and ESR dating. *Archaeometry* **28**, 202-205.

Reviewer
R. Grün

Error analysis and modelling of double saturating exponential dose response curves from SAR OSL dating

G.W. Berger [1] and R. Chen [2]

[1] Desert Research Institute, 2215 Raggio Parkway, Reno, NV 89512, USA.
 (e-mail: glenn.berger@dri.edu)
[2] School of Physics and Astronomy, Tel-Aviv University, Tel-Aviv, 69978, Israel

_____

Abstract
Increasingly observed in single-aliquot regenerative dose (SAR) optically stimulated luminescence (OSL, also termed photon stimulated luminescence or PSL) dating studies of sedimentary quartz are dose response curves that at high doses are not satisfied by a single saturating exponential (SSE) regression model. Commonly these can appear to be satisfied by a SSE+Linear (E+L) regression model, but some authors have proposed that a double saturating exponential (DSE) model would more closely fit the observed dose response curves (DRCs), especially in the region of highest applied doses. As error analysis for SAR equivalent dose (D_e) values derived from a DSE model is not yet available through the widely available Risø supplied software (Analyst), we present here a regression and error analysis scheme for DSE SAR data, and also a simple charge traffic model that generates approximate DSE dose responses. To illustrate results from our error analysis, we employ two SAR high dose data sets for fine-grain quartz, and compare graphically the SSE, E+L and DSE fits for each data set. These comparisons show clearly that such data are more closely fitted by a DSE regression than by the other two models. This result, and the charge traffic model, lend validity to the physical reality of DSE regression models, and have implications for quartz SAR dating of older sediments.

Introduction
Recently there has been increasing interest in the use of the high dose part of quartz SAR DRCs to estimate burial ages from unheated sediments (e.g., Lowick and Preusser, 2011; Lowick et al., 2010a, 2010b; Murray et al., 2007, 2008; Pawley et al., 2008, 2010; Timar et al., 2010). Most of these reports are concerned with how to assess the accuracy of equivalent dose (D_e) values derived from such DRCs because some of the age estimates are lower than expected based on indirect, independent evidence. Although these studies considered several possible explanations for the observed age estimate

discrepancies (e.g. validity of independent ages, accuracy and/or variation of estimates of past water concentration, soundness of SAR self-consistency tests), part of the discussion in these reports of high-dose DRCs concerns the best-fit model, though the examples of age underestimations illustrated by, for example, Lowick and Preusser (2011) do not depend on the fitting model.

Berger (2010) summarized several published reports of high dose TL (thermoluminescence) and SAR DRCs that appeared to be best fitted by an E+L regression model. Additional examples of high dose SAR DRCs that appeared to be best fitted by an E+L model are reported in chapter 5 of Bøtter-Jensen et al. (2003). All of these examples used relatively few dose points and did not extend the DRC to very high (many kGy) doses. Berger (2010) noted that some authors (Wintle and Murray, 2006; Murray et al., 2007, 2008) considered that a DSE model would also fit their DRCs. Recently, Lowick and Preusser (2011), Lowick et al. (2010a), and Pawley et al. (2010) showed that a DSE model would fit some of their DRCs as well as an E+L model up to applied doses of ~1 kGy. These authors used the E+L model to calculate interpolated D_e values from the high dose region of the relevant DRCs because an interpolation and error analysis scheme for calculation of D_e values from a DSE model was not available to them.

We present here a regression and error analysis scheme for DSE DRCs, as well as a simple charge traffic model that simulates DSE DRCs. The equations for our DSE regression and error analysis scheme are extensions of those of Berger (2010) for the E+L model. Using the nomenclature of Berger (2010), the DSE model is

$$f = a(1-e^{-bx}) + c(1-e^{-dx}) \qquad (1)$$

where the second SSE could manifest a second set of charge traps having a different saturation level than the type of traps represented in the first SSE. The

essential equations are outlined below. We illustrate the results with two fine-grain-quartz SAR data sets.

Regression to Obtain Parameters *a*, *b*, *c* and *d*

The nomenclature of Berger (2010) is followed here. Using the weighted least-squares principle, we wish to minimize

$$S = \sum_i w_i(y_i - f_i)^2 \qquad (2)$$

where f is defined by Eq 1 and the weights for each y_i value (L/T, SAR normalized OSL) are $1/\sigma_y^2$, and σ^2 is the absolute error variance in each L/T ratio. Corrected (Berger, 2011) Eq 12 of Berger (2010)

$$\Delta A = \left([\sqrt{W}U]^t[\sqrt{W}U]\right)^{-1}\left([\sqrt{W}U]^t[\sqrt{W}Y^*]\right)$$

for the iterative calculation of the best-fit parameters, is used to derive best-fit parameters θ (*a*, *b*, *c* and *d* herein) by iteration, employing the elements of the matrices $\sqrt{W}U$ and $\sqrt{W}Y^*$, where matrix elements $u_{ik} = \partial f_i/\partial\theta_k$. The elements of the weighted matrices are as follows:

$$wu_a = (1 - e^{-bx_i})\sqrt{w_i},$$

$$wu_b = ax_i e^{-bx_i}\sqrt{w_i},$$

$$wu_c = (1 - e^{-dx_i})\sqrt{w_i},$$

$$wu_d = cx_i e^{-dx_i}\sqrt{w_i},$$

$$wy^* = [y_i - a(1 - e^{-bx_i}) - c(1 - e^{-dx_i})]\sqrt{w_i}.$$

Solution for D_e and Error in D_e

We solve for D_e by using the Newton-Raphson iterative procedure (e.g. McCalla, 1967) applied to the equation

$$f' = y_0 - a(1-e^{-bx}) - c(1-e^{-dx}) \qquad (3)$$

because f ' = 0 when x = D_e , where $y_0 = L_0/T_0$, the L/T ratio for the 'natural' measurement.

As in Berger (2010), we calculate two components of the variance in D_e. The first arises from the variance in y_0 and is obtained by using the repeated steps of Berger (2010) and his equation 16

$$\sigma_{D_e}^2(y_0) = \left[\left(D_e' - D_e''\right)/2\right]^2$$

The second error component in D_e arises from the scatter of data about the best-fit curve and from the errors in the parameters *a*, *b*, *c*, and *d*, as well as from the covariances of these errors. We calculate this

second component by use of an extension to equation 4 of Berger (1990). This equation is

$$\Delta^2 = \frac{V^t \cdot SIG \cdot V}{|\partial f/\partial D_e|^2},$$

where SIG is the symmetric error matrix (the variance-covariance matrix) and equals VAR·(I)$^{-1}$, I is the information matrix of Berger et al. (1987), and VAR is a scalar.

$$VAR = \frac{\sum_i w_i(y_i - f_i)^2}{N-5}$$

where N is the number of L/T data points including the origin.

Thus, in the equation for Δ^2, $\frac{\partial f}{\partial D_e} = (abe^{-bD_e} + cde^{-dD_e})$, with f given by Eq 1 above. The elements of the above transpose matrix $V^t = (\partial f/\partial a, \partial f/\partial b, \partial f/\partial c, \partial f/\partial d)$ are then as follows:

$$\frac{\partial f}{\partial a} = (1 - e^{-bx}),$$

$$\frac{\partial f}{\partial b} = axe^{-bx},$$

$$\frac{\partial f}{\partial c} = (1 - e^{-dx}),$$

$$\frac{\partial f}{\partial d} = cxe^{-dx},$$

and are evaluated with x = D_e.

To complete our calculation of the second component of the error in D_e (that arising from the scatter of data about the best-fit DRC and errors in fitting parameters), we need the elements of the above symmetric matrix I. These elements are derived from Eq 3 of Berger (2010)

$$I_{k,s} = \sum_i \frac{1}{f_i^2}\frac{\partial(f_i)}{\partial\theta_k} \cdot \frac{\partial(f_i)}{\partial\theta_s}$$

and are as follows (with $1/f_i^2$ replaced by w_i as in Berger, 2010):

$$I_{aa} = \sum_i w_i(1 - e^{-bx_i})^2,$$

$$I_{ab} = I_{ba} = \sum_i w_i(1 - e^{-bx_i})(ax_i e^{-bx_i}),$$

$$I_{ac} = I_{ca} = \sum_i w_i(1 - e^{-bx_i})(1 - e^{-dx_i}),$$

$$I_{ad} = I_{da} = \sum_i w_i(1 - e^{-bx_i})(cx_i e^{-dx_i}),$$

$$I_{bb} = \sum_i w_i(ax_i e^{-bx_i})^2,$$

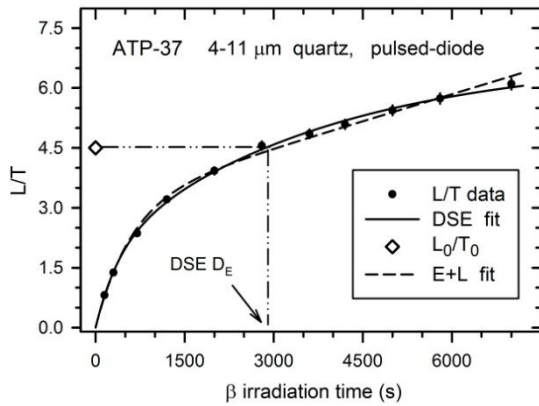$$I_{bc} = I_{cb} = \sum_i w_i(ax_i e^{-bx_i})(1 - e^{-dx_i}),$$

Figure 1: *Comparison of DSE and E+L best-fit DRCs for sample ATP-37. Error bars for L/T data here and in Fig. 2 are ±1σ. Here and for sample ATP-18, a preheat of 240°C(10s) was employed. The dose rate for the beta source used is 0.12 Gy/s.*

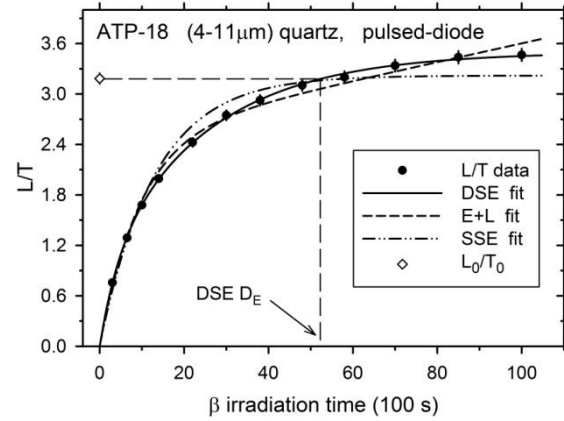$$I_{bd} = I_{db} = \sum_i w_i (a x_i e^{-b x_i})(c x_i e^{-d x_i}) \ ,$$

$$I_{cc} = \sum_i w_i (1 - e^{-d x_i})^2 \ ,$$

$$I_{cd} = I_{dc} = \sum_i w_i (1 - e^{-d x_i})(c x_i e^{-d x_i}) \ ,$$

$$I_{dd} = \sum_i w_i (c x_i e^{-d x_i})^2 \ .$$

The two calculated components of the variance in D_e are then summed as in Eq 15 of Berger (2010) to yield the total variance in D_e.

$$\sigma^2_{D_e} = \sigma^2_{D_e}(y_0) + \sigma^2_{D_e}(\theta)$$

Comparison of Results from Data Sets
The DRC for the data set ATP-37 of Berger (2010) showed an apparently near linear component superimposed upon an SSE. The top of Berger's (2010) Fig. 2 compared the best-fit SSE with the best-fit E+L regressions. In Fig. 1 here we use the same data set to compare the E+L and DSE fits to this high-dose data set. While the differences in the DRCs might appear slight to the eye, they are significant. The 'Fit' value (weighted sums of squares of residuals) for the E+L fit is 1.42, and that for the DSE (0.80) is significantly smaller. Such a Fit value provides a more discriminating estimate of the fit of a regression model than does the less sensitive R^2 value often cited by authors. In this example, the estimated D_e from the DSE regression is smaller (2860 ±190 s) than that from the E+L regression (3060±260 s) as expected, though not statistically different at 1σ.

Figure 2: *Comparison of SSE, E+L and DSE best fit DRCs for sample ATP-18. The dose rate of the beta source used is 0.12 Gy/s.*

Table 1: *SAR data for sample ATP-18*

Dose (s)	L/T
Natural	3.184 ± 0.068
300	0.757 ± 0.016
650	1.290 ± 0.028
1000	1.679 ± 0.036
1400	1.994 ± 0.043
2200	2.425 ± 0.052
3000	2.747 ± 0.059
3800	2.925 ± 0.063
4800	3.103 ± 0.067
5800	3.201 ± 0.069
7000	3.338 ± 0.074
8500	3.437 ± 0.074
10000	3.465 ± 0.074
recup'n	0.005 ± 0.002
Recycle	0.84 ± 0.03

Note: These L/T ratios are from the screen display of *Analyst* v3.24, which truncates errors to the third decimal place.

Our second high dose data set (sample ATP-18, Table 1) is also from a 4-11 μm fraction of purified quartz (extracted using H_2SiF_6 acid), apparently having (as does sample ATP-37) only a fast component of quartz OSL. In Fig. 2 we compare the best fit regression curves of SSE, E+L and DSE for the ATP-18 data. Clearly, the SSE model is inappropriate. The SSE Fit value is 3.08. The E+L model evidently provides a better fit, having a Fit value of 1.69, and yielding a D_e value of 6280±700 s.

However, the DSE model provides the closest fit (Fit = 0.40), and the D_e value is smaller (5270±550 s) as expected, with a smaller error. It is clear that a DSE model is more appropriate for these data than is an E+L model, though the error analysis reveals that the difference in estimates of D_e values is not statistically significant at 1σ for these data.

A Charge-traffic Model for a DSE Dose Response
One of the conceptual problems with the use of the E+L regression model is that, although it can represent a realistic physical process under application of high laboratory doses (trap creation superimposed upon filling of existing charge traps, Berger (2010) and citations therein), it is difficult to understand how this model can represent what occurs naturally over geological time scales under much lower dose rates. Notwithstanding, Lowick and Preusser (2011, pg.40) found no empirical evidence in their experiments "to suggest that the presence of a high dose linear response in quartz OSL is only a laboratory generated phenomenon and does not occur in the natural environment". In general, however, several authors (cited in the introduction above) have assumed that a DSE model is more physically realistic, but that in most cases an E+L model provides sufficiently accurate estimates of D_e values from the high dose region of the DRC (and our example data do not show otherwise, at the 1σ level of significance). A particular difficulty has been in conceptualizing a specific charge traffic process or set of competing processes that could account for a DSE dose response.

One envisioned process (e.g. Wintle and Murray, 2006) is that the second SSE term in Eq 1 above manifests the filling of a set of traps different from those manifested by the first SSE term. But what is meant by 'different', and what other charge transport processes might account for such DRCs? Ankjærgaard et al. (2006) provided experimental evidence for discrimination among possible charge traffic schemes of OSL (and TL). They employed optically stimulated electron emission (OSE) and OSL in a comparative study of some natural dosimeters (NaCl, quartz and feldspar). Whereas OSL (and TL) manifest the end results of both charge eviction and charge recombination, OSE reflects only charge eviction. They observed that OSE from quartz and feldspar decays more quickly than OSL, and suggested that this difference manifests the recombination step, possibly involving a delay in the recombination process of OSL (and TL). They also observed differences in the OSE and OSL DRCs, which they attribute to "a dose dependent change in luminescence recombination efficiency", associated
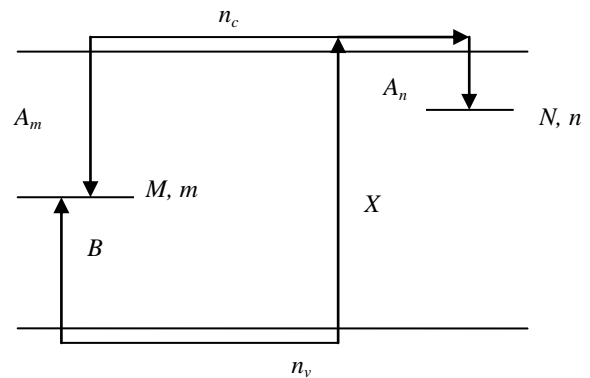

Figure 3: *Charge traffic model used in this study.*

with OSL. However, Ankjærgaard et al. (2009) observed no significant differences in DRC shapes resulting from similar OSE and OSL experiments on additional quartz samples, inferring that luminescence recombination is not generally the main limit to the dose range of DRCs. Furthermore, Lowick et al. (2010a, p. 983) inferred from their experiments with quartz OSL that the high dose behaviour in the DRC could be accounted for by "a change in competition for electrons between the UV recombination centres whose emission is seen through the detection window and recombination centres that do not emit in this spectral region...".

In the context of the above, we present a simple charge traffic model that produces statistically good DSE DRCs, but that involves only one electron trapping state (N) and one type of recombination centre (M), and (significantly) a 'long' relaxation time. The model is sketched in Fig. 3. Parameters N (cm^{-3}) and M (cm^{-3}) denote the concentrations of the traps and centres, respectively, and n (cm^{-3}) and m (cm^{-3}) their corresponding instantaneous occupancies. The parameters n_c (cm^{-3}) and n_v (cm^{-3}) are the instantaneous concentrations of free electrons and holes, respectively. Parameter B (cm^{3}s^{-1}) is the probability coefficient for capturing free holes in the recombination centre. Parameter A_m (cm^{3}s^{-1}) is the recombination probability coefficient for electrons to recombine with holes in the centres, and A_n (cm^{3}s^{-1}) the probability coefficient for retrapping. Parameter X (cm^{-3}s^{-1}) is the rate of production of electron-hole pairs by the irradiation, which is proportional to the excitation dose rate. If an excitation of constant intensity takes place for a period of time t_D (s), the total number of pairs produced is $X \cdot t_D$ (cm^{-3}), which is proportional to the total applied dose D.

The set of rate equations governing the process is:

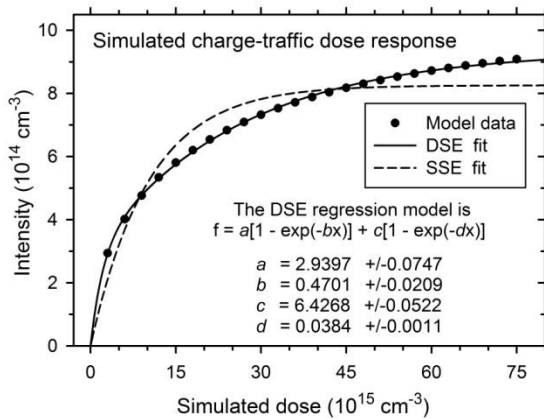$$\frac{dn}{dt} = A_n(N - n)n_c \qquad (4)$$

Figure 4: *Simulated charge traffic dose response and best fit regressions. These regressions (from SigmaPlot v11.2) use 1/y² weighting.*

$$\frac{dm}{dt} = B(M - m)n_v - A_m m n_c \qquad (5)$$

$$\frac{dn_v}{dt} = X - B(M - m)n_v \qquad (6)$$

$$\frac{dn_c}{dt} = \frac{dm}{dt} + \frac{dn_v}{dt} - \frac{dn}{dt} \qquad (7)$$

In order to demonstrate the behaviour of the dependence of excitation on the dose, we have chosen the following set of parameters: $N=10^{15}$ cm^{-3}; $M=10^{16}$ cm^{-3}; $n_0=m_0=0$; $B=10^{-9}$cm^{3}s^{-1}; $A_n=2\times10^{-9}$ cm^{3}s^{-1}; $A_m=10^{-7}$cm^{3}s^{-1} and $X=3\times10^{15}$cm^{-3}s^{-1}. The simulated irradiations had varying lengths between 3 and 75 s, which produced the different 'applied' doses.

In order to simulate the excitation process properly, each excitation was followed by a long relaxation time during which, the remaining holes in the valence band were captured in the recombination centre. The remaining electrons in the conduction band were either retrapped or recombined with holes in the centre during the relaxation time. The final concentrations of electrons following excitation and relaxation were recorded. Note that in this simple model of one trap and one recombination centre, the concentrations of electrons in the trap and holes in the centre must be equal at the end of the relaxation time.

The recorded values of the final trap occupancy are assumed to represent the luminescence signal. In the case of TL, this represents the area under the glow peak measured following the excitation and relaxation. For OSL it represents the integral under the decay curve, again, following excitation and relaxation.

The results of the simulation with the above mentioned set of parameters are shown in Fig. 4. The analysis shows that the DSE regression model yields significantly better agreement with the simulated results than does the single saturating exponential (SSE) model. The exponential constants *b* and *d* in the regression model (Eq 1) seem to be associated with the processes of electron capture in traps (probability coefficient A_n) and of holes in centres (probability coefficient *B*) during the excitation and relaxation.

Conclusions

A scheme for regression and estimation of total variance in paleodose (D_e) values derived from SAR OSL experiments is presented for a double saturating exponential (DSE) dose response curve (DRC). With real SAR data from two samples of fine-silt quartz given relatively high laboratory doses, the DSE regression model provides a better fit to the DRCs than does the saturating exponential plus linear (E+L) regression model. Additionally, the estimated errors in the respective D_e values are smaller (as expected because of the better regression fits) than otherwise. The implication of the DSE behaviour of real sample data for OSL dating by SAR is that there is an upper limit to the OSL of the DRCs and this provides one constraint on the maximum age for such dating that would not be encountered if an E+L model represented actual dose response in nature. The upper age limit is likely constrained by the behaviour represented by the second SSE, which may be related to hole-capture behaviour.

Our simple charge traffic model simulates closely a DSE dose response. This simple model has only a single electron trapping state and a single type of recombination centre, and incorporates a 'long' relaxation time as per the experimental procedure. While this simple charge traffic model appears to provide a sufficient match to the observed best-fit DSE regression, other more complicated charge traffic models might also produce similar results. Nonetheless, the two exponents in our simple model may be associated with the two processes of filling of traps and centres, but the full process is likely to be more complicated.

References

Ankjærgaard, C., Murray, A.S., Denby, P.M., Bøtter-Jensen, L. (2006) Measurement of optically and thermally stimulated electron emission from natural minerals. *Radiation Measurements* **41**, 780-786.

Ankjærgaard, C., Murray, A. S., Denby, P. M., Jain, M. (2009). Using optically stimulated electrons from quartz for the estimation of natural doses. *Radiation Measurements* **44**, 232-238.

Berger, G.W. (1990) Regression and error analysis for a saturating-exponential-plus-linear model. *Ancient TL* **8**, 23-25.

Berger, G.W. (2010) Estimating the error in equivalent dose values obtained from SAR. *Ancient TL* **28**, 55-66.

Berger, G.W. (2011) Errata: Estimating the error in equivalent dose values obtained from SAR. *Ancient TL* **29**, 51.

Berger, G.W., Lockhart, R.A., Kuo, J. (1987) Regression and error analysis applied to the dose response curves in thermoluminescence dating. *Nuclear Tracks and Radiation Measurements* **13**, 177-184.

Bøtter-Jensen, L., McKeever, S. W. S., Wintle, A. G. (2003). *Optically Stimulated Luminescence Dosimetry*. Elsevier.

Lowick, S.E., Preusser, F. (2011) Investigating age underestimation in the high dose region of optically stimulated luminescence using fine grain quartz. *Quaternary Geochronology* **6**, 33-41.

Lowick, S.E., Preusser, F., Wintle, A.G. (2010a) Investigating quartz optically stimulated luminescence dose-response curves at high doses. *Radiation Measurements* **45**, 975-984.

Lowick, S.E., Preusser, F., Pini, R., Ravazzi, C. (2010b) Underestimation of fine grain quartz OSL dating towards the Eemian: comparison with palynostratigraphy from Azzano Decimo, northeastern Italy. *Quaternary Geochronology* **5**, 583-590.

McCalla, T.R. (1967) *Introduction to Numerical methods and FORTRAN Programming*. John Wiley & Sons, New York, 351pp.

Murray, A. S., Svendsen, J. I., Mangerud, J., Astakhov, V. I. (2007) Testing the accuracy of quartz OSL dating using a known-age Eemian site on the river Sula, northern Russia. *Quaternary Geochronology* **2**, 102-109.

Murray, A. S., Buylaert, J-P., Henriksen, M., Svendsen, J-I., Mangerud, J. (2008) Testing the reliability of quartz OSL ages beyond the Eemian. *Radiation Measurements* **43**, 776-780.

Pawley, S.M., Bailey, R.M., Rose, J., Moorlock, B.S.P., Hamblin, R.J.O., Booth, S.J., Lee, J.R. (2008) Age limits on Middle Pleistocene glacial sediments from OSL dating, north Norfolk, UK. *Quaternary Science Reviews* **27**, 1363-1377.

Pawley, S.M., Toms, P., Armitage, S.J., Rose, J. (2010) Quartz luminescence dating of Anglian Stage (MIS 12) fluvial sediments: comparison of SAR age estimates to the terrace chronology of the Middle Thames valley, UK. *Quaternary Geochronology* **5**, 569-582.

Timar, A., Vandenberghe, D., Panaiotu, E.C., Panaiotu, C.G., Necula, C., Cosma, C., van den Haute, P. (2010) Optical dating of Romanian loess using fine-grained quartz. *Quaternary Geochronology* **5**, 143-148.

Wintle, A. G., Murray, A. S. (2006) A review of quartz optically stimulated luminescence characteristics and their relevance in single-aliquot regeneration dating protocols. *Radiation Measurements* **41**, 369-391.

Reviewer

F. Preusser

Core drilling of Quaternary sediments for luminescence dating using the Dormer Drillmite[TM]

Kennedy Munyikwa[1], Matt Telfer[2,*], Ian Baker[3], Chelsea Knight[4]

[1]Centre for Science, Athabasca University, 1 University Drive, Athabasca, Alberta, T8N 1T3, Canada (email: kenm@athabascau.ca)
[2] School of Geography and the Environment, University of Oxford, South Parks Road, Oxford, OX1 3QY, UK
[3]Dormer Soil Samplers, 4 Mayfield St, Murwillumbah South, NSW 2484, Australia
[4]Earth and Atmospheric Sciences, University of Alberta, Edmonton, Alberta, T6G 2E3, Canada.
*Present address - School of Geography, Earth and Environmental Sciences, University of Plymouth, 7 Kirby Place, Drake Circus, Plymouth, PL4 8AA, UK

Abstract

The coring of buried Quaternary deposits using a Dormer Drillmite[TM] auger permits the extraction of samples for luminescence dating from depths of up to 20 m. The unit is powered hydraulically and features portability as one of its main advantages. While a range of other power drilling methods have been used successfully for sample collection in a number of luminescence dating studies, there is a dearth of literature that describes such drilling methods in detail. The absence of such information belies the importance of sampling methods in luminescence dating. This contribution aims to play a role in addressing that deficit. The basic operational features of the Drillmite[TM] are outlined and we share some experiences we have had coring with the unit. Adaptations that can be made to the equipment to suit different circumstances are explored. The advantages and drawbacks of core drilling at depth for luminescence dating are also briefly examined.

Introduction

A primary requirement for sediments intended for luminescence dating is that the mineral grains to be analyzed should not be exposed to light from the time they are initially buried up till the point they are exposed to the stimulating source during measurement. This restriction necessitates the adoption of special precautions during sample collection and a number of procedures have been devised over the years. Such measures include sampling at night (e.g. Aitken, 1998; Lian and Roberts, 2006), but this inconvenient. In settings where the sediment is sufficiently indurated, an alternative approach is to cut out a block of sample from the depositional unit being investigated for subsequent sub-sampling in light-controlled conditions (Aitken, 1998; Lian and Roberts, 2006, Ó Cofaigh et al., in press). A sampling approach that has become a method of choice because of its ease and relative guarantee for retrieval of an unadulterated sample is to insert an opaque pipe made of metal or plastic into a freshly prepared profile face (Aitken, 1998). Once retrieved, the pipe is immediately capped on both ends with an opaque and preferably moisture-tight seal. At the laboratory, sediment at the ends of the pipe is removed and the sample for OSL measurements is taken from the central portion of the pipe.

A feature that characterizes all these methods, however, is that the profile face being sampled has to be directly accessible. There are numerous advantages to working from exposed sedimentary profiles; the lithostratigraphy can be readily recorded, lateral continuity of the units being sampled can be checked, and samples can be taken precisely from locations that either avoid specific problems (e.g. evidence of bioturbation) or target certain features (e.g. sand lenses). There are occasions, however, when direct access to the entire sedimentary profile under investigation may not be possible and studies of aeolian dunes for paleoenvironmental reconstruction provide good examples of such cases. In central and northern Alberta, Canada, for instance, several luminescence dating investigations have been completed on aeolian dunes that mantle the postglacial landscape (e.g. Wolfe et al., 2002, 2004, 2007; Munyikwa et al., 2011). The dunes in the region attain heights of up to 20 m (Halsey et al., 1990) but, in the majority of cases, sample extraction has been confined to the upper 2-3 m. Consequently, reconstructions performed using the results can only

be viewed as partial records of the chronology contained in the aeolian deposits.

Because natural full-depth sediment exposures in unconsolidated sandy sediments are often scarce, researchers have frequently sought alternative approaches. In many regions, road cuttings in Quaternary sediments have become prime locations for sampling (e.g. Bateman et al., 2004; Spencer and Owen, 2004; Porat and Botha, 2008; McIntosh et al., 2009). Alternatively, investigators have excavated pits to gain access to buried depositional units (e.g. Stokes et al., 1997; Wolfe et al., 2004; Munyikwa et al., 2011), but with obvious practical limitations to the depth that can be attained in sand. Occasionally, backhoe diggers have also been used (e.g. Lomax et al., 2003) to cut open profiles but this approach can be costly and is potentially damaging if practised in environmentally sensitive areas.

The most obvious solution to these problems would be to sample remotely down augered boreholes and recover intact sediment, suitable for luminescence dating. A study of the literature will show that a range of devices have been employed to drill holes to extract samples for dating. Very few of the operational procedures used, however, have been described in detail, making it difficult for new investigators who face similar situations to benefit from the experiences of others. This contribution focuses on the use of one such sampling device: the Dormer Drillmite™ auger. We describe field experiences we have had over a number of sampling seasons using the system in order to provide practical advice for other workers who might be interested in using the unit or a comparable method. We also assess the merits and drawbacks of the system compared to other methods of sample collection.

Extracting samples for luminescence dating by drilling
The extraction of coarse grained samples for luminescence dating by drilling is not a new concept. Early attempts include studies by Nanson et al. (1992, 1998) who used a hand auger to collect aeolian dune and playa sediments from depths of up to 8 m. In these studies, samples were recovered by quickly placing the auger bit with the sample into an opaque plastic bag where the sample was removed and packed (Nanson et al., 1992, 1998). A potential problem associated with this approach is the possibility of exposing the sample to light during transfer from the hole to the opaque container. Subsequently, other users (e.g. Rodnight et al., 2005; Tooth et al., 2007) overcame this problem by fixing a sampling tube to the auger once the required sampling depth had been reached. Wallinga and van

der Staay (1999) described a hand operated device (the Van der Staay suction-corer) for extracting samples from waterlogged sands which also addressed the risk of exposure to light. With the Van der Staay corer, samples are extracted from depths of up to 7 m in a removable coring tube which is sealed afterwards and transported to the lab for analysis.

Vibracorers, which penetrate sediment through a vibratory motion as opposed to rotary or percussion action employed in conventional drilling, have also been used to collect samples for luminescence dating in some studies (e.g. Rittenour et al., 2003). Normally, vibracoring retrieves samples as continuous cores in hollow tubing and this shields the sediment from sunlight upon extraction from the hole.

A mechanized bailer-drilling unit originally described by Oele et al. (1983) has been used in a number of luminescence dating studies to extract sediment cores from depths in excess of 35 m (e.g. Törnqvist et al., 2000; Wallinga et al., 2004; Busschers et al., 2008). Cores obtained using the mechanical bailer are retrieved in 1 m long PVC pipe sections which ensures that the sediments are not exposed to sunlight above ground. Working at greater depths, Preusser et al. (2002) utilized a large drilling rig to drill a triple-lined hole and attained a depth of 140 m in very large linear dunes of the Wahiba Sands of Oman. Sample recovery from the cores in that study, however, was limited to 50 - 80%.

In a study that sought to adapt the drilling method to the depth of drilling in order to maximize sample recovery in aeolian sequences, Bristow et al. (2005; 2007) employed a combination of drilling rigs to extract luminescence dating samples from various positions within the interior of an aeolian dune. In the upper 10 m, a percussion auger mounted on a truck was used. For dune depths beyond 10 m, however, a Dormer sand auger equipped with an auger flight housed in a counter rotating core barrel was found to be more appropriate (Bristow et al., 2007). Other vehicle mounted rigs that have been used to extract samples for luminescence dating include the Geoprobe® Systems coring outfit (e.g. Zlotnik et al., 2007). Geoprobe® rigs generally operate on a direct push mechanism which is a variant of the percussive drilling mode. As with other methods described above, the Geobrobe® samples are extracted from the ground in opaque tubing in which they may be transported to the lab.

A number of recent studies (e.g. Chase and Thomas, 2006, 2007; Telfer and Thomas, 2006, 2007; Telfer et al., 2009; Stone and Thomas, 2008; Burrough et al.,

2007; Burrough and Thomas, 2008), have provided very brief accounts of the usage of a lightweight, portable, hydraulic auger: the Dormer Engineering Drillmite[TM]. This system combines three important characteristics of a convenient sampling technique which can be inferred from the different methods described above, viz.: portability, operational ease, and the ability to extract samples from depths beyond a few metres. Its use as well as that of the other drilling methods cited above demonstrates that any method that extracts samples intended for luminescence dating by coring at depth has to address three attendant problems:

- the method has to avoid exposure of the samples to sunlight during transfer from the drilled hole to the container;
- it has to be possible to determine the stratigraphic context and precise depth at which the sample is being collected;
- there has to be some means available of ascertaining the integrity (for dating purposes) of the sediment at the base of the hole prior to sampling.

All three topics are discussed below with reference to the Drillmite[TM].

Sample extraction by augering with the Dormer Drillmite[TM] auger
Manufactured by Dormer Engineering (www.dormersoilsamplers.com) of New South Wales, Australia, the Dormer Drillmite[TM] is a portable 6 HP diesel or gasoline driven hydraulic unit for powering augers (Fig. 1 and Fig. 2). The unit weighs around 60 kg and, hence, operating it far from a vehicle would generally be ill-advised. The system is manoeuvrable by two people but if only one operator is available to auger, it should be noted that the sand drill bit provided with the kit can be operated manually without hydraulic power very successfully, and depths of at least 8 m have been attained by a single operative (Telfer, in press).

The Drillmite[TM] outfit comes with components specifically designed for luminescence dating. However, as discussed below, some adaptations may need to be made to suit specific circumstances. Drill bits can be selected for soil, sand or clay substrate (Fig. 3b and c). The targeted depth is reached by augering and removing successive sediment cores of about 30 cm at a time. As the working depth increases, the drill stem is extended by attaching additional aluminum or steel extension rods (Fig. 3f and Fig. 4a).
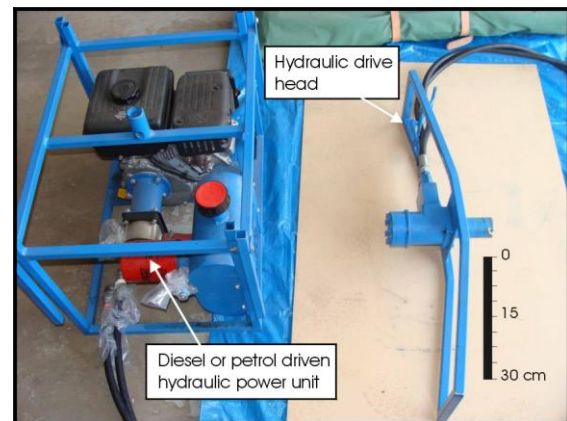
Figure 1. *The Dormer Drillmite[TM] hydraulic power unit and drive head.*

Figure 2. *Though the Drillmite[TM] can be operated by a single person, it is often convenient for two persons to work in partnership.*

Generally, as long as the working depth is above the water table, holes drilled in moist dune sands maintain their walls well. Telfer et al. (2009) utilised a Drillmite[TM] to auger into the clayey silt and sand pan floor sediments at Witpan, southwestern Kalahari, which included the extraction of at least 1 m of sediment below the water table; it seems unlikely such a strategy would work so well in unconsolidated dune sands. Conversely, in very dry, fine sands, a hole collapse is possible, and if this occurs at depth, there is the risk that an auger or sampling head may be lost. If extraction of sands with the auger head proves difficult (i.e. the drill bit fails to retain the sediment load), Stone and Thomas (2008) successfully mitigated the problem by pouring water down the hole to moisten the sands to improve cohesion. Although this strategy inevitably results in some movement of sediment down the hole, if allowed sufficient time (usually overnight) to percolate into the dune, successful extraction of both
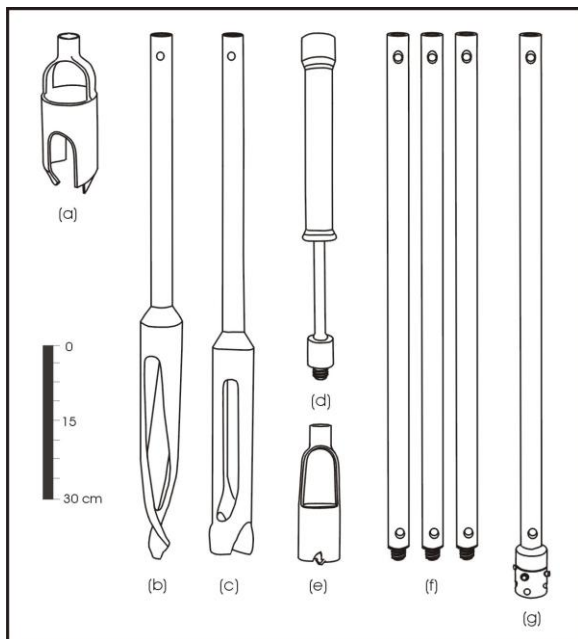
Figure 3. *Depending on the scope of the intended work, a range of accessories for the Drillmite^TM can be acquired from Dormer, including: (a) a large diameter drill bit; (b) a drill bit for clayey formations; (c) a drill bit for sandy formations; (d) slide hammer for driving sampling modules into the ground; (e) hole shaver for cleaning the bottom of the hole; (f) extension rods for increasing the working depth, and (g) adaptors for attaching sampling modules (see Figure 5) at the end of the drill stem.*


Figure 4. *(a) The desired working depth is reached by removing successive sediment cores of about 30 cm at a time followed by reinserting the drill stem into the hole and drilling further. Once the desired depth is reached, the drill bit is replaced by a hole shaver which is used to remove loose sediment from the bottom of the hole. (b) A sampling module is then attached at the end of the drill stem and hammered into the ground using a slide hammer. The sample is extracted from the hole by pulling the drill stem vertically upwards.*

the detrital material and intact sands was eventually possible. In even moderately dry dune sands, digging a working platform into the damper sub-surface sands (at ~1 m depth in the southwestern Kalahari) from which to auger helped reduce the effects of hole collapse. Experience in both the Kalahari and Canada has also shown that it may be advantageous at times to case the upper 20-30 cm of the hole using a large diameter acrylonitrile butadiene styrene (ABS) plastic pipe (Fig. 4). This provides a firm working lip and prevents fallback from disturbed sediment during the repeated insertion and retrieval of the drill stem from the hole.

Extracting a core sample without exposure to light
Once the desired sampling depth is reached, samples for luminescence dating are collected using stainless steel push tubes supplied by Dormer (Fig. 5a). The tubes were designed following suggestions from John Magee (formerly Australian National University), Gifford Miller (University of Colorado) and Gerald Nanson (Wollongong University). A drive adaptor

(Fig. 3g and Fig. 5) couples the push tube to the bottom extension rod (Fig. 4b) and a slide hammer (Fig. 3d) is used to drive the sampling tube into the ground as illustrated in Fig. 4b.

The reusable sampling push tubes, as provided by the manufacturer, are convenient, but they may have a number of significant disadvantages for some users. They are heavy once filled with sediment, and even allowing for the discarding of light-contaminated ends, the amount of material collected is excessive in sand-rich sediments. Given the increasing focus on intensive sampling strategies (e.g. Telfer and Thomas, 2007; Telfer, in press), this imposes serious logistic limitations, particularly if international transport is required. For investigators who do not have their own dating lab, the use of reusable sampling tubes would necessitate the transfer of the samples to other packaging prior to dispatch to the dating lab. To avoid such laborious routines,

Figure 5. *Sample extraction modules are attached at the end of the lowermost extension rod using a drive adaptor as illustrated above. (a) Dormer supplies reusable stainless steel pipes for use in sample collection. (b) Because it is sometimes necessary to send collected samples to other labs for analysis, it may be more practical to collect samples using single-use ABS plastic pipes. (c) To permit on-site pre-inspection of a subsurface unit, a see-through acrylic pipe can be attached at the end of the drill stem and a sample extracted as in (b).*
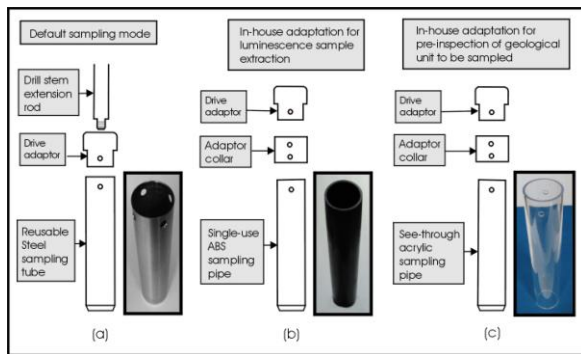
Munyikwa and Knight (2010) have fashioned a disposable push tube using a 6 cm diameter by 30 cm long ABS plastic pipe (Fig. 5b). With a wall about 4 mm thick, the pipe is rigid enough to withstand the force imparted by the slide hammer. To enhance penetration into the substrate being sampled, the ABS pipe can be sharpened. Shorter pipes can be used to reduce weight if desired. To attach the ABS push tube to the drive adapter which attaches to the drill stem, an additional collar may need to be designed (Fig. 5b). The push tube is fixed to the collar using a detachable through bolt. When the sample is retrieved from the hole, the push tube is detached by removing the through bolt after which the tube is sealed on both ends. Field experiences show that both the steel and ABS sampling tubes are generally efficient and, unless waterlogged or extremely dry, the sediment stays firmly in the tube during extraction from the hole.

Alternatively, in the quartz sand dominated dunes of the southwestern Kalahari, Telfer and colleagues (Telfer and Thomas, 2006, 2007; Telfer et al., 2009; Telfer, in press) have subsampled from the steel sample head with a 5 cm diameter by 12.5 cm length black plastic pipe in the field in a large opaque plastic bag. After discarding the outermost sediment in the steel sampling head, the plastic tube can be pushed into the sampling head by hand, and is then carefully extracted when full. This subsample is then capped,

and treated exactly as a sample taken from an exposure would be; that is, the ends are still considered light-contaminated and discarded.

Determining the stratigraphic context of a sample
The most significant drawback for sampling by deep coring is that the investigator is not able to see, in-situ, the depositional unit being sampled, nor its immediate stratigraphic context. This is significant not only in terms of ensuring that the correct unit is being sampled, but also because, ideally, samples for luminescence dating should be collected from a substrate that is homogenous within a radius of at least 30 cm (Aitken, 1998). This is particularly important if in-situ dosimetry is not available.

At the most basic level, stratigraphic positioning is achieved by careful monitoring of the depth that the sample is taken from. This is easily attained by counting extension rods, and it may prove useful to mark the individual rods with tape at suitable intervals (e.g. 20 cm) to aid measurement. The Drillmite™ kit comes with a shaver which can be used to retrieve loose sediment from the base of the hole (Fig. 3e). Shaving the hole base enables the determination of the precise depth at which samples are extracted.

Telfer and Thomas (2007) attempted to minimize any potential complications to dosimetry imposed by the blind nature of sampling down a borehole by measuring dose rate in-situ with a gamma spectrometer lowered down the borehole. This has been done by constructing a steel casing for a 2" NaI gamma scintillometer (necessitating a separate calibration of the instrument to reflect the changing geometries of measurement), which allows the probe to be lowered to the base of the hole.

Ascertaining the integrity of the sample
It is critical that the auger or sampling head is inserted into the borehole cleanly; this becomes increasingly challenging with depth as it becomes necessary for practitioners to lower the auger in several separate stages. Any contact with the sidewalls during the lowering of the auger or sampling unit will result in sediment dropping to the base of the hole. Evidence that this does indeed occur comes from the slow widening of the hole evident at the surface, as well as a slower rate of penetration at depth (as the removal of material knocked down the hole reduces the overall rate of augering). Such down-hole contamination threatens the integrity of the luminescence sample.

To determine the degree of disruption of the sample, Munyikwa and Knight (2010) have devised a

transparent detachable push tube that can be attached at the end of the drill stem in place of the sampling push tube (Fig. 5c). A sample is extracted by driving the transparent tube into the subsurface unit using the slide hammer and pulling it out. While this method may preserve stratification in some compact sediments, it has been noted that the penetration of the pipe into the formation sometimes disrupts fine bedding. Increasing the internal diameter of the sampling tube appears to help preserve the stratification better. Dormer also supplies a similar sampling module which comprises a steel tube with a removable internal transparent plastic sleeve for extracting samples for pre-inspection. Alternatively, a split tube sampler can be used to achieve the same objective.

Single-grain studies on samples removed from auger holes suggests that down-hole incorporation of young grains is minimal if augering is conducted carefully (Telfer, in press), and if hole collapse does occur, careful examination of dose distributions may be useful in identifying the problem (Telfer and Thomas, 2007). It is advisable, however, to avoid windy days for augering, as it becomes increasingly difficult to ensure that the auger and extensions rods are held vertically before lowering into the hole.

Advantages and drawbacks: case examples of the Drillmite[TM] in use

Canada
Munyikwa and Knight (2010) have used the Drillmite[TM] extensively in central and northern Alberta, Canada to extract samples for luminescence dating in aeolian dunes from depths up to 20 m. It is well accepted that the region was glaciated by the Laurentide Ice Sheet during the Last Glacial Maximum (Dyke et al., 2002, 2003). However, the scarcity of radiocarbon bearing material has rendered the timing of the retreat of the ice sheet from the region difficult to constrain. Wolfe et al. (2007) and Munyikwa et al. (2011) have proposed the use of luminescence chronology from postglacial aeolian dunes in the region as an alternative time constraint for the retreat of the ice sheet. The rationale of this approach is that eolian deposition denotes an ice-free landscape and that dune emplacement commenced in the immediate aftermath of the recession of the ice sheet, prior to colonisation by vegetation. Accordingly, sampling using the Dormer Drillmite[TM] has been targeted at the bottoms of the dunes.

Results show that sampling with the Drillmite[TM] can be performed rapidly, with hole completion rates of 10-15 m in a day being easily attained. The manufacturer specifies that the Drillmite[TM] can drill to depths of up to 60 m, but work in Alberta shows

that a limiting factor is the mechanism employed to hoist the drill stem in and out of the drill hole. With manual hoisting, one can work down to a depth of 15-20 m. Beyond this depth the weight of the drill stem becomes prohibitive and a powered hoisting system becomes necessary. Also worth knowing is that occasionally, especially when working in clayey substrates, the sampling module can become stuck. As advised by the manufacturer, an effective remedy in such cases is to use a car jack to provide vertical leverage to the segment of the drill stem projecting at the surface.

Southwestern Kalahari
Prior to the application of the Drillmite[TM] during field campaigns in 2002 and 2004, sampling of the huge semi-active southwestern Kalahari linear dunefield in southern Africa had only been possible via surface pits and occasional road-cuts (e.g. Stokes et al., 1997), or even scarcer deep exposures resulting from mine workings (Bateman et al., 2003). Such studies confirmed the homogenous nature of most Kalahari dunes, with stratigraphy often absent or very poorly preserved. The crucial drawback of sampling at depth, namely that intact internal stratigraphy cannot be observed, is thus perhaps less critical in this area than it might be in some other regions. However, the Drillmite[TM] offered the opportunity for full-depth profiling of dunes selected by criteria other than convenience, and as a result intensive, localized sampling was carried out to re-assess the implications of the more opportunistic sampling that had gone before. Over 100 samples were collected from a small region, and these revealed previously unconfirmed spatial variation in preservation of dune sediments (Telfer and Thomas, 2006, 2007). For the first time, full-depth profiling of the dunes allowed studies that would simply not have been possible without the use of a rapid augering system capable of working in unconsolidated sandy substrates. The studies enabled a rigorous assessment of the preservation potential of linear dunes of the Kalahari over timescales longer than the most recent major period of dune mobilization (at around 15 – 9 ka). More recently, systematic augered OSL sampling of dunes has also been used to test geomorphic models of dune formation, sometimes in combination with Ground-Penetrating Radar (GPR) (e.g. Hollands et al., 2006; Telfer, in press).

The rapidity with which sampling can be carried out has some implications for the use of technologies such as the Drillmite[TM]; the rate of augering possible during fieldwork, and hence the numbers of samples collected, probably far outstrips the capabilities of many laboratories for subsequent analysis. An efficient team of two field operatives might

comfortably collect more than 100 samples in a week's fieldwork; a work schedule which might subsequently keep many laboratories busy for up to a year. Although laboratory procedures such as standardized growth curves (Roberts and Duller, 2004) have been explored for handling such large volumes of samples (e.g. Telfer et al., 2008), those planning large scale augering surveys are likely to have to consider issues of quantity and quality more carefully than ever.

Summary

A cursory literature review will show that, on many occasions, luminescence dating investigators have been confronted with situations when remote sampling of geological units that are not directly accessible has been imperative. In such instances, drilling to reach the targeted units has offered an attractive solution and a range of drilling devices have been employed. The Dormer Drillmite[TM] presents a viable alternative for such sampling work because of its field portability as well as its ability to sample deeper than many other outfits of comparable size. The system comes with equipment specifically designed for extracting samples for luminescence dating and various adaptations can be made to suit specific circumstances.

In addition to being capable of sampling deeper than would be possible unaided, sampling devices such as the Drillmite[TM] are also able to yield large numbers of samples over relatively short periods of time. The high sample acquisition rates will hopefully encourage the development of accelerated analytical protocols if excessive backlogs are to be avoided in luminescence dating laboratories.

All in all, these possibilities widen the prospects for paleoenvironmental studies that use records from Quaternary deposits.

Acknowledgements

References

Aitken, M.J. (1998) *An Introduction to Optical Dating*. Oxford University Press, Oxford.

Bateman, M.D., Thomas, D.S.G., Singhvi, A.K. (2003) Extending the aridity record of the Southwest Kalahari: current problems and future perspectives. *Quaternary International* **111**, 37-49.

Bateman, M.D., Holmes, P.J., Carr, A.S., Horton, B.P., Jaiswal, M.J. (2004) Aeolianite and barrier dune construction spanning the last two glacial-interglacial cycles from the southern Cape coast, South Africa. *Quaternary Science Reviews* **23**, 1681-1698.

Bristow, C.S., Lancaster, N., Duller, G.A.T. (2005) Combining ground penetrating radar surveys and optical dating to determine dune migration in Namibia. *Journal of the Geological Society, London* **162**, 315-321.

Bristow, C.S., Duller, G.A.T., Lancaster, N. (2007) Age and dynamics of linear dunes in the Namib Desert. *Geology* **35**, 555-558.

Burrough, S.L., Thomas, D.S.G. (2008) Late Quaternary lake-level fluctuations in the Mababe Depression: Middle Kalahari palaeolakes and the role of Zambezi inflows. *Quaternary Research* **69**, 388-403.

Burrough, S.L., Thomas, D.S.G., Shaw, P.A., Bailey, R.M. (2007) Multiphase Quaternary highstands at Lake Ngami, Kalahari, northern Botswana. *Palaeogeography, Palaeoclimatology, Palaeoecology* **253**, 280-299.

Busschers, F.S., Van Balen, R.T., Cohen, K.M., Kasse, C., Weerts, H.J.T., Wallinga, J., Bunnik, F.P.M. (2008) Response of the Rhine-Meuse fluvial system to Saalian ice-sheet dynamics. *Boreas* **37**, 377-398.

Chase, B.M., Thomas, D.S.G. (2006) Late Quaternary dune accumulation along the western margin of South Africa: distinguishing forcing mechanisms through the analysis of migratory dune forms. *Earth and Planetary Science Letters* **251**, 318-333.

Chase, B.M., Thomas, D.S.G. (2007) Multiphase late Quaternary aeolian sediment accumulation in western South Africa: Timing and relationship to palaeoclimatic changes inferred from the marine record. *Quaternary International* **166**, 29-41.

Dyke, A.S., Andrews, J.T., Clark, P.U., England, J.H., Miller, G.H., Shaw, J., Veillette, J.J. (2002) The Laurentide and Inuitian ice sheets during the Last Glacial Maximum. *Quaternary Science Reviews* **21**, 9-31.

Dyke, A.S., Moore, A.J., Robertson, L. (2003) Deglaciation of North America. *Geological Survey of Canada, Open File* **1574**.

Halsey, L.A., Catto, N.R., Rutter, N.W. (1990) Sedimentology and development of parabolic dunes, Grand Prairie dune field, Alberta. *Canadian Journal of Earth Sciences* **12**, 1762 -1772.

Hollands, C.B., Nanson, G.C., Jones, B.G., Bristow, C.S., Price, D.M., Pietsch, T.J. (2006) Aeolian-fluvial interaction: evidence for Late Quaternary channel change and wind-rift linear dune formation in the northwestern Simpson Desert, Australia. *Quaternary Science Reviews* **25**, 142-162.

Lian, O., Roberts, R.G. (2006) Dating the Quaternary: progress in luminescence dating of sediments. *Quaternary Science Reviews* **25**, 2449–2468.

Lomax, J., Hilgers, A., Wopfner, H., Grün, R., Twidale, C.R., Radtke, U. (2003) The onset of dune formation in the Strzelecki Desert, South Australia. *Quaternary Science Reviews* **22**, 1067-1076.

McIntosh, P.D., Price, D.M., Eberhard, R., Slee, A.J. (2009) Late Quaternary erosion events in lowland and mid-altitude Tasmania in relation to climate change and first human arrival. *Quaternary Science Reviews* **28**, 850-872.

Munyikwa, K., Knight, C.E. (2010) Deep vertical coring of eolian dune structures for luminescence dating. *Proceedings of the Prairie Summit – Joint Conference of the CAG, CCA, CGRG and CRSS. Regina, Saskatchewan, Canada, June 2010,* pp 221-224.

Munyikwa, K., Feathers, J.K., Rittenour, T. M., Shrimpton, H.K. (2011) Constraining the retreat of the Laurentide ice sheet from western Canada using luminescence ages from postglacial aeolian dunes. *Quaternary Geochronology* **6**, 407-422.

Nanson, G.C., Chen, X. Y., Price, D.M. (1992) Lateral migration, thermoluminescence chronology and color variation of longitudinal dunes near Birdsville in the Simpson desert, Central Australia. *Earth Surface Processes and Landforms* **17**, 807-819.

Nanson, G.C., Callen, R.A., Price, D.M. (1998) Hydroclimatic interpretation of Quaternary shorelines on South Australian playas. *Palaeogeography, Palaeoclimatology, Palaeoecology* **144**, 281-305.

Ó Cofaigh, C., Telfer, M.W., Bailey, R.M., Evans, D.J.A. (in press) Late Pleistocene chronostratigraphy and ice sheet limits, southern Ireland. *Quaternary Science Reviews*, doi:10.1016/j.quascirev.2010.01.011.

Oele, E., Apon, W., Fischer, M.M., Hoogendoorn, R., Mesdag, C.S., De Mulder, E.F.J., Overzee, B., Sesören, A., Westerhoff, W.E. (1983) Surveying The Netherlands: sampling techniques, maps and their applications. *Geologie en Mijnbou* **62**, 355-372.

Porat, N., Botha, G. (2008) The luminescence chronology of dune development on the Maputaland coastal plain, southeast Africa. *Quaternary Science Reviews* **27**, 1024-1046.

Preusser, F., Radies, D. Matter, A., (2002) A 160,000-year record of dune development and atmospheric circulation in southern Arabia. *Science* **296**, 2018-2020.

Rittenour, T.M, Ronald J., Goble, R.J., Blum, M.D. (2003) An optical age chronology of late Pleistocene fluvial deposits in the northern lower Mississippi valley. *Quaternary Science Reviews* **22**, 1105-1110.

Roberts, H.M., Duller, G.A.T. (2004) Standardised growth curves for optical dating of sediment using multiple-grain aliquots. *Radiation Measurements* **38**, 241-252.

Rodnight, H., Duller, G.A.T., Tooth, S., Wintle, A.G. (2005) Optical dating of a scroll-bar sequence on the Klip River, South Africa, to derive the lateral migration rate of a meander bend. *The Holocene* **15**, 802-811.

Spencer, J.Q., Owen, L.A. (2004) Optically stimulated luminescence dating of Late Quaternary glaciogenic sediments in the upper Hunza valley: validating the timing of glaciation and assessing the dating methods. *Quaternary Science Reviews* **23**, 175-191.

Stokes, S., Thomas, D.S.G., Shaw, P.A. (1997) New chronological evidence for the nature and timing of linear dune development in the southwest Kalahari Desert. *Geomorphology* **20**, 81-93.

Stone, A.E.C., Thomas, D.S.G. (2008) Linear dune accumulation chronologies from the southwest Kalahari, Namibia: challenges of reconstructing late Quaternary palaeo-environments from aeolian landforms. *Quaternary Science Reviews* **27**, 1667-1681.

Telfer, M.W., Thomas, D.S.G. (2006) Complex Holocene lunette dune development, South Africa: Implications for paleoclimate and models of pan development in arid regions. *Geology* **34**, 853-856.

Telfer, M.W., Thomas, D.S.G. (2007) Late Quaternary linear dune accumulation and chronostratigraphy of the southwestern Kalahari: implications for aeolian palaeoclimatic reconstructions and predictions of future dynamics. *Quaternary Science Reviews* **26**, 2617-2630.

Telfer, M.W., Bateman, M.D., Carr, A.S., Chase, B.M. (2008) Testing the applicability of a standardized growth curve (SGC) for quartz OSL dating: Kalahari dunes, South African coastal dunes and Florida dune cordons. *Quaternary Geochronology* **3**, 137-142.

Telfer, M.W., Thomas, D.S.G., Parker, A.G., Walkington, H., and Finch, A.A. (2009) Optically Stimulated (OSL) dating and paeloenvironmental studies of pan (playa) sediment from Witpan, South Alfrica. *Palaeogeography, Palaeoclimatology, Paleoecology* **273**, 50-60.

Telfer, M.W. (In press). Growth by extension, and reworking, of a southwestern Kalahari linear dune. *Earth Surface Processes and Landforms* DOI: 10.1002/esp.2140

Tooth, S., Rodnight, H., Duller, G. A. T., McCarthy, T. S., Marren, P. M., Brandt, D. (2007). Chronology and controls of avulsion along a mixed bedrock-alluvial river. *Geological Society of America Bulletin* **119**, 452-461.

Törnqvist, T.E., Wallinga, J., Murray, A.S., De Wolf, H., Cleveringa, P., De Gans, W. (2000) Response of the Rhine-Meuse system (west central Netherlands) to the last Quaternary glacio-eustatic cycles: a first assessment. *Global and Planetary Change* **27**, 89-111.

Wallinga J., van der Staay, J. (1999) Sampling in water logged sands with a simple hand operated corer. *Ancient TL* **17**, 59-61.

Wallinga, J., Törnqvist, T.E., Busschers, F.S., Weerts, H.J.T. (2004) Allogenic forcing of the late Quaternary Rhine-Meuse fluvial record: the interplay of sea-level change, climate change and crustal movements. *Basin Research* **16**, 535-547.

Wolfe, S.A., Ollerhead, J., Lian, O.B. (2002) Holocene aeolian activity in south-central Saskatchewan and the southern Canadian Prairies. *Geographie physique et Quaternaire* **56**, 215-227.

Wolfe, S.A., Huntley, D.J., Ollerhead, J. (2004) Relict Late Wisconsinan dune fields of the Northern Great Plains, Canada. *Geographie physique et Quaternaire* **58**, 323-336.

Wolfe, S.A., Paulen R.C., Smith I.R., Lamothe M. (2007) Age and paleoenvironmental significance of Late Wisconsinan dune fields in the Mount Watt and Fontas River map areas, northern Alberta and British Columbia. *Geological Survey of Canada, Current Research* 2007-B4, 1-10

Zlotnik, V.A., Burbach, M., Swinehart J., Bennet, D., Fritz, S.C., Loope, D.B., Olaguera F. (2007) Using Direct-Push methods for Aquifer characterisation in Dune-Lake environments of the Nebraska Sand Hills. *Environmental and Engineering Geoscience* **XIII**, 205-216.

Reviewer
J. Wallinga

Thesis Abstracts

_____

Author: Christina Ankjærgaard
Thesis Title: Understanding optically stimulated charge movement in quartz and feldspar using time-resolved measurements
Grade: Ph.D.
Date: May 2010
Supervisors: Mayank Jain (Risø DTU), Stig Steenstrup (University of Copenhagen)
Address: Radiation Research Division, Risø Natural Laboratory for Sustainable Energy, Technical University of Denmark (DTU)

Optically stimulated luminescence (OSL) from quartz and feldspar is widely used in luminescence dating and other forms of retrospective dosimetry. In order to develop new techniques to extend the general applicability of the dating technique it is important to understand the processes of luminescence generation in these minerals. OSL is a multi-step process involving charge excitation, transport, and recombination; using time-resolved OSL (TR-OSL) one has the possibility to directly examine the role of charge transport and recombination in luminescence emission.

The thesis is a compilation of 9 published articles, an introduction, and a summary chapter. It first delves into three main methodological developments, namely, (i) research and development of the equipment for TR-OSL measurements, (ii) finding the best method for multiple-exponential analysis of a TR-OSL curve, and (iii) optimisation of the pulsing configuration for the best separation of quartz OSL from a mixed quartz-feldspar sample. It then proceeds to study the different charge transport mechanisms subsequent to an optical stimulation pulse in quartz and feldspars over time scales covering 9 orders of magnitude (tens of nanoseconds to tens of seconds).

The results obtained for quartz conclude that the main lifetime component in quartz represents an excited state lifetime of the recombination centre, and the more slowly decaying components on the millisecond to seconds time scale arise from charge recycling through shallow traps.

Feldspars are studied using IR, green and blue stimulations and a combination of TR-OSL and time-resolved exo-electron (TR-OSE) emission techniques. It is shown that irrespective of composition, the TR-OSL shape of feldspars are very similar to each other, and that the lifetime of the excited state of the recombination centre is not important on the time scales of our measurements. The measurements give insights into the relative roles of an IR excited state (IR resonance), band tail states and the conduction band during charge transport in feldspars. Phonon assisted transport and tunnelling from the band tail states are characterised for the first time. It is shown that the band tail route favours production of a signal with a lower fading rate. Based on these results a comprehensive model of feldspar luminescence is developed, and different methods are proposed to deal with the long standing problem of anomalous fading.

This thesis is available as a PDF on the Ancient TL web site www.aber.ac.uk/ancient-tl

Author : Dorthe Pflanz
Thesis Title: Coastal Development in Eastern Kamchatka – results from OSL Dating, Remote Sensing and Fieldwork
Grade: Ph.D.
Date: November 2010
Supervisors: J.Kley (IGW – FSU, Jena), C.Dullo (IFM – Geomar, Kiel), M. Krbetschek (TU Freiberg), R.Freitag (BGR - Hannover)
Address: Institut of Applied Geosciences, Burgweg 11, D-07743 Jena, Germany

In this study, OSL dating was used to determine uplift rates on an active margin. The Kamchatka subduction zone is one of the most active convergent margins in the world. The Pacific Plate is subducting beneath the Kurile-Kamchatka margin since the Eocene, today with an average rate of 7.9 cm/a. Thereby the Peninsula is involved by strong neotectonic activities. Indicators of these activities on the eastern coastline are deformed Pleistocene sediments; recent thrust faulting and high uplifted marine terraces on different levels. The different levels of the elevated terraces points to variant uplift rates within the peninsula.

The geological records of marine terraces are the depositional and erosional remains of former

shorelines, so they are records of the former sea level. Along active continental margins, the marine terraces reflect the interplay between sea level oscillations and surface uplift. Dated marine terraces record the time of sea level high stands, but although the vertical crustal movement.

In the working area, 3-5 paleoshorelines are mapped via remote sensing. The aim of this study was to quantify the uplift from paleoshorelines by calculating uplift rates on OSL ages of marine terrace. Sediment age determination was carried out at the luminescence laboratory Freiberg (TU Freiberg /Inst. of Appl. Physics). The source materials of the marine terraces are mainly volcanic sediments. Because of a high fraction of magnetic material in these sediments, magnetic separation of sieved carbonate and organics free sediment fraction was used as an additional step for purifying the quartz within a procedure which furthermore applied feldspar flotation, density separation and HF etching. A single-aliquot regenerative-dose (SAR) procedure was used for palaeodose determination. It was necessary to add different hot-bleach treatments to the standard SAR-procedure based on a series of experiments. Broad statistical approaches on dose distribution in such samples from marine sedimentary environment have been applied.

This study presents the first quantitative results about age and uplift on the eastern coast of Kamchatka.

Author: Christopher Lüthgens
Thesis Title: The age of Weichselian main ice marginal positions in north-eastern Germany inferred from Optically Stimulated Luminescence (OSL) dating.
Grade: PhD
Date: February 2011
Supervisors: Margot Böse (Freie Universität), M. Krbetschek (TU Freiberg, single aliquot OSL), F. Preusser (University of Bern, single grain OSL)
Address: Freie Universität Berlin, Department of Earth Sciences, Berlin, Germany

During the past 130 years, classification of the Weichselian Pleniglacial in north-eastern Germany was mainly based on morphostratigraphical interpretations. In general, three main ice marginal positions are distinguished. The ice advance to the southernmost, relatively weakly developed ice marginal position of the Brandenburg phase has traditionally been ascribed to the Last Glacial Maximum (LGM) of the Scandinavian Ice Sheet (SIS). The Frankfurt phase is usually interpreted as a halt during the downmelting of the glacier. The most prominent ice marginal position in north-eastern Germany is that of the Pomeranian phase.

Owing to the absence of recent geochronological data of the Weichselian ice advances, the commonly used ages of ice marginal positions are only estimates or are based on extrapolations from ^{14}C ages of underlying organic sediments. However, during the past few years a number of studies have been conducted to set up a chronology based on geochronometrical data. In this study fluvioglacial sediments from outwash plains associated with the Brandenburg phase and the Pomeranian phase were dated by means of Optically Stimulated Luminescence (OSL) of single aliquots and single grains of quartz. Recently, additional ages from Surface Exposure Dating (SED) of erratic boulders using cosmogenic ^{10}Be have been published. To compare the results from these different approaches, the type and position of the sampled material within the glacial landscape system have to be considered. Consequently, different geomorphological processes are datable using either OSL or SED techniques. Therefore a process-based interpretation for numerical ages from OSL and SED in glacigenic landscapes is introduced.

From the results of the OSL analyses from the Brandenburg and Pomeranian phases as well as a thorough reassessment of the available ^{10}Be exposure ages, a synthesis was achieved in terms of ice dynamics and ice retreat patterns during Marine Isotope Stage (MIS) 2. One of the main findings is the evidence for a twofold LGM, with the older phase (LGM-1) corresponding to the Brandenburg phase, which was dated to <34 ka (maximum age), and the younger phase (LGM-2) represented by the Pomeranian phase, which was dated to 20.1 ±1.6 ka (initial formation of outwash plains) and 19.4 ±2.4 ka (final sedimentation of sandur sediments).

The first Weichselian deglaciation pattern for north-eastern Germany was established, based on results from numerical dating methods, and the last glacial-interglacial cycle was dated for the first time from a terrestrial Saalian-Eemian-Weichselian sedimentary sequence in the research area.

This thesis is available from: http://www.diss.fu-berlin.de/diss/receive/FUDISS_thesis_000000022882

Author: Femke Davids
Thesis Title: Optical dating of hurricane activity in New England, USA.
Grade: PhD
Date: September 2010
Supervisors: Geoff Duller, Helen Roberts
Address: Institute of Geography & Earth Sciences, Aberystwyth University, UK

This study has investigated hurricane activity during the late Holocene on the southern New England coastline (USA) by means of optical dating of overwash layers deposited in coastal salt marshes and ponds. Three alternative optical dating methods were investigated; quartz OSL, K-feldspar IRSL and the subtraction method. Both quartz and K-feldspar ages agree with independent age constraints (^{14}C) and are suitable for dating young hurricane overwash deposits. The majority of ages (53) were consistent with stratigraphical control.

Although K-feldspar ages were more precise, quartz was the most practicable method for this project considering the limited availability of sand grains in general, and K-feldspar specifically, in the thin overwash layers in this region. The signal analysis for quartz was improved by applying early background (EBG). A test on 13 samples demonstrated that EBG: 1) reduced the proportional influence of medium and slow components to the net signal; 2) reduced recuperation values; and 3) reduced the over dispersion value for some samples.

The D_e distributions from the overwash sediments showed both well bleached and heterogeneously bleached samples. The finite mixture model and the central age model were applied to determine the optical age. A modern analogue (hurricane Bob, AD 1991) was, moreover, very accurately and precisely dated with quartz minerals.

This study shows that determining the dose rate in heterogeneous sediment is challenging. Sensitivity analyses on the external dose rates demonstrated that variability in water content produced the most uncertainty in dose rates. Therefore, it is important to know not only the water content of the overwash layer but also of the bracketing layers. Furthermore, it was demonstrated that the dose rate should be corrected for organic content when samples have more than 5% organic content. Additionally, this study showed that X-ray core scanning can have an effect on the optical age of a sediment. Depending on the dose rate of the sediment, this could produce a significant offset to young geological samples, e.g. late Holocene.

The optical dating results from the six coastal salt marshes and ponds along the southern New England coastline roughly indicate a period of activity between 2 - 1 ka before AD 2000 (*ca.* 6 major events), a period of less activity between 1 - 0.5 ka before AD 2000, and a period of high activity (*ca.* 7 major events) during the last 0.5 ka.

Author: Lara Wacha
Thesis Title: Luminescence dating of loess from the island of Susak in the Northern Adriatic Sea and the "Gorjanović loess section" from Vukovar in eastern Croatia.
Grade: PhD
Date: May 2011
Supervisors: Manfred Frechen (LIAG), Goran Durn (University of Zagreb)
Address: Leibniz Institute for Applied Geophysics (LIAG), Hannover, Germany

Loess-palaeosol sequences are an excellent high-resolution archive for palaeoenvironmental changes. They hide information about the past climate and climatic changes. To be able to reconstruct the palaeoenvironment it is common practice to investigate these deposits with a multidisciplinary approach. A detailed and reliable geochronology is mandatory to be able to interpret the results of such investigations.

The aim of this study was to establish a reliable chronological framework of loess-palaeosol sequences from Croatia. In Croatia two major loess regions can be distinguished, the North Adriatic loess region related to the river Po in North Italy and its tributaries and the Danube loess region in eastern Croatia. From both regions the most representative loess-palaeosol sequences were selected for investigations; the loess-palaeosol sequence on the island of Susak, where up to 90 m of Quaternary deposits, predominantly loess and loess derivatives were determined, and the "Gorjanović loess section" in Vukovar, which is the matter of scientific interest since the last centuries. These two genetically similar but in many ways different remains of climatic fluctuations during the Pleistocene were selected to be the topic for a detailed multi-proxy research for this PhD.

This geochronological framework is the first step in high-resolution investigations which is in progress. The dating was performed using infrared stimulated luminescence (IRSL) dating method, which is the method of choice for dating of Quaternary aeolian

deposits, as well as radiocarbon dating. Throughout this PhD several luminescence dating protocols were used; the multiple aliquot additive (MAAD) dose protocol which is a somewhat old-fashioned protocol was used for polymineral fine grain material separated from the loess from Susak for an easier correlation with older published data in this area; the single aliquot regenerative (SAR) protocol which is a widely used measuring protocol, with fading tests and fading corrections performed on the measured samples as well, to obtain more reliable dating results. For the "Gorjanović loess section" the post-IR IRSL protocol, which is a modified SAR protocol developed recently for dating of older deposits (Middle Pleistocene) was introduced. This protocol has the advantage that it can overcome the performance of fading tests and fading corrections since in this protocol more stable luminescence signals from feldspars are registered.

Using the above mentioned laboratory measuring protocols which were supported by numerous experiments and performance tests good and reliable geochronological frameworks for the sections under study were established. The results from the loess-palaeosol sequences on Susak show us that a very detailed record correlating to OIS5 (and possibly OIS6 or older) is preserved, unique in this region. Furthermore, based on the dating results as well as mineralogical and geochemical investigations the three tephra layers were correlated to South Italian volcanic provinces. The luminescence dating results are supported by the radiocarbon dating as well. The "Gorjanović loess section" is an example of the penultimate glacial- last interglacial – last glacial period (OIS6 – OIS2), as seen from the dating results, and can easily be correlated to similar loess-palaeosol sections in the region.

In this thesis a detailed and reliable chronological framework of prominent loess-palaeosol sequences in Croatia is established as well as a milestone for a stratigraphy of Quaternary deposits in Croatia.

Bibliography
Compiled by Daniel Richter

From 1st November 2010 to 30th April 2011

Alappat, L., Tsukamoto, S., Singh, P., Srikanth, D., Ramesh, R., and Frechen, M. (2010). Chronology of Cauvery delta sediments from shallow subsurface cores using elevated-temperature post-IR IRSL dating of feldspar. *Geochronometria* **37,** 37-47.

Alexanderson, H., Landvik, J. Y., Molodkov, A., and Murray, A. S. (2011). A multi-method approach to dating middle and late Quaternary high relative sea-level events on NW Svalbard - A case study. *Quaternary Geochronology* **6,** 326-340.

Alexanderson, H., Landvik, J. Y., and Ryen, H. T. (2011). Chronology and styles of glaciation in an inter-fjord setting, northwestern Svalbard. *Boreas* **40,** 175-197.

Andreucci, S., Clemmensen, L. B., and Pascucci, V. (2010). Transgressive dune formation along a cliffed coast at 75 ka in Sardinia, Western Mediterranean: a record of sea-level fall and increased windiness. *Terra Nova* **22,** 424-433.

Anselmetti, F. S., Drescher-Schneider, R., Furrer, H., Graf, H. R., Lowick, S. E., Preusser, F., and Riedi, M. A. (2010). A ~180,000 years sedimentation history of a perialpine overdeepened glacial trough (Wehntal, N-Switzerland). *Swiss Journal of Geosciences* **103,** 345-361.

Arbogast, A. F., Bigsby, M. E., DeVisser, M. H., Langley, S. A., Hanson, P. R., Daly, T. A., and Young, A. R. (2010). Reconstructing the age of coastal sand dunes along the northwestern shore of Lake Huron in Lower Michigan: Paleoenvironmental implications and regional comparisons. *Aeolian Research* **2,** 83-92.

Armitage, S. J., Jasim, S. A., Marks, A. E., Parker, A. G., Usik, V. I., and Uerpmann, H.-P. (2011). The Southern Route "Out of Africa": Evidence for an Early Expansion of Modern Humans into Arabia. *Science* **331,** 453-456.

Baartman, J. E. M., Veldkamp, A., Schoorl, J. M., Wallinga, J., and Cammeraat, L. H. (2011). Unravelling Late Pleistocene and Holocene landscape dynamics: The Upper Guadalentín Basin, SE Spain. *Geomorphology* **125,** 172-185.

Barham, L., Phillips, W. M., Maher, B. A., Karloukovski, V., Duller, G. A. T., Jain, M., and Wintle, A. G. (2011). The dating and interpretation of a Mode 1 site in the Luangwa Valley, Zambia. *Journal of Human Evolution* **60,** 549-570.

Bateman, M. D., Carr, A. S., Dunajko, A. C., Holmes, P. J., Roberts, D. L., McLaren, S. J., Bryant, R. G., Marker, M. E., and Murray-Wallace, C. V. (2011). The evolution of coastal barrier systems: a case study of the Middle-Late Pleistocene Wilderness barriers, South Africa. *Quaternary Science Reviews* **30,** 63-81.

Benito, G., Thorndycraft, V. R., Rico, M. T., Sánchez-Moya, Y., Sopeña, A., Botero, B. A., Machado, M. J., Davis, M., and Pérez-González, A. (2011). Hydrological response of a dryland ephemeral river to southern African climatic variability during the last millennium. *Quaternary Research* **75,** 471-482.

Berger, G. W., Doran, P. T., and Thomsen, K. J. (2010). Single-grain and multigrain luminescence dating of on-ice and lake-bottom deposits at Lake Hoare, Taylor Valley, Antarctica. *Quaternary Geochronology* **5,** 679-690.

Bertran, P., Bateman, M. D., Hernandez, M., Mercier, N., Millet, D., Sitzia, L., and Tastet, J.-P. (2011). Inland aeolian deposits of south-west France: facies, stratigraphy and chronology. *Journal of Quaternary Science* **26,** 374-

388.

Beukema, S. P., Krishnamurthy, R. V., Juyal, N., Basavaiah, N., and Singhvi, A. K. (2011). Monsoon variability and chemical weathering during the late Pleistocene in the Goriganga basin, higher central Himalaya, India. *Quaternary Research* **75,** 597-604.

Bianca, M., Catalano, S., De Guidi, G., Gueli, A. M., Monaco, C., Ristuccia, G. M., Stella, G., Tortorici, G., Tortorici, L., and Troja, S. O. (2011). Luminescence chronology of Pleistocene marine terraces of Capo Vaticano peninsula (Calabria, Southern Italy). *Quaternary International* **232,** 114-121.

Biswas, R. H., Morthekai, P., Gartia, R. K., Chawla, S., and Singhvi, A. K. (2011). Thermoluminescence of the meteorite interior: A possible tool for the estimation of cosmic ray exposure ages. *Earth And Planetary Science Letters* **304,** 36-44.

Blain, S., Guibert, P., Prigent, D., Lanos, P., Oberlin, C., Sapin, C., Bouvier, A., and Dufresne, P. (2011). Combined dating methods applied to building archaeology: The contribution of thermoluminescence to the case of the bell tower of St Martin's church, Angers (France). *Geochronometria* **38,** 55-63.

Boroda, R., Amit, R., Matmon, A., Team, A., Finkel, R., Porat, N., Enzel, Y., and Eyal, Y. (2011). Quaternary-scale evolution of sequences of talus flatirons in the hyperarid Negev. *Geomorphology* **127,** 41-52.

Bright, J., Kaufman, D. S., Forman, S. L., McIntosh, W. C., Mead, J. I., and Baez, A. (2010). Comparative dating of a Bison-bearing late-Pleistocene deposit, Térapa, Sonora, Mexico. *Quaternary Geochronology* **5,** 631-643.

Buylaert, J.-P., Huot, S., Murray, A. S., and Van Den Haute, P. (2011). Infrared stimulated luminescence dating of an Eemian (MIS 5e) site in Denmark using K-feldspar. *Boreas* **40,** 46-56.

Campbell, M. C., Fisher, T. G., and Goble, R. J. (2011). Terrestrial sensitivity to abrupt cooling recorded by aeolian activity in northwest Ohio, USA. *Quaternary Research* **75,** 411-416.

Campos, S. S., Almeida, G. M., Cardoso, L. X., de Lima, L. L., Carlos, A., and de Souza, S. O. (2010). Thermoluminescent dose reconstruction using quartz extracted from unfired buildings. *Journal of Physics: Conference Series* **249,** 012031.

Cao, Y., Li, S., Yao, M., and Zhang, H. (2010). Thermoluminescence of quartz from Shihu gold deposit, western Hebei province, China: some implications for gold exploration. *Central European Journal of Geosciences* **2,** 433-440.

Carvalho Jr., A. B., Guzzo, P. L., Sullasi, H. L., and Khoury, H. J. (2010). Effect of particle size in the TL response of natural quartz sensitized with high gamma dose. *Journal of Physics: Conference Series* **249,** 012027.

Chen, Y., Li, Y., Zhang, Y., Zhang, M., Zhang, J., Yi, C., and Liu, G. (2011). Late Quaternary deposition and incision sequences of the Golmud River and their environmental implications. *Quaternary International* **236,** 48-56.

Chithambo, M. L., Sane, P., and Tuomisto, F. (2011). Positron and luminescence lifetimes in annealed synthetic quartz. *Radiation Measurements* **46,** 310-318.

Christiansson, M., Bernhardsson, C., Mattsson, S., and Rääf, C. L. (2011). Using an optimised OSL single-aliquot regenerative-dose protocol for low-dose retrospective dosimetry on household salt. *Radiation Protection Dosimetry* **144,** 584-587.

Cunningham, A. C., and Wallinga, J. (2010). Selection of integration time intervals for quartz OSL decay curves. *Quaternary Geochronology* **5,** 657-666.

Dunajko, A. C., and Bateman, M. D. (2010). Sediment provenance of the Wilderness barrier dunes, southern Cape coast, South Africa. *Terra Nova* **22,** 417-423.

Ellwein, A. L., Mahan, S. A., and McFadden, L. D. (2011). New optically stimulated luminescence ages provide evidence of MIS3 and MIS2 eolian activity on Black Mesa, northeastern Arizona, USA. *Quaternary Research* **75,** 395-398.

Elmejdoub, N., Mauz, B., and Jedoui, Y. (2011). Sea-level and climatic controls on Late Pleistocene coastal aeolianites in the Cap Bon peninsula, northeastern Tunisia. *Boreas* **40,** 198-207.

Erkens, G., Hoffmann, T., Gerlach, R., and Klostermann, J. (2011). Complex fluvial response to Lateglacial and Holocene allogenic forcing in the Lower Rhine Valley (Germany). *Quaternary Science Reviews* **30,** 611-627.

Fan, A., Li, S.-H., and Li, B. (2011). Observation of unstable fast component in OSL of quartz. *Radiation Measurements* **46,** 21-28.

Frechen, M., Ellwanger, D., Hinderer, M., Lämmermann-Barthel, J., Neeb, I., and Techmer, A. (2010). Late Pleistocene fluvial dynamics in the Hochrhein Valley and in the Upper Rhine Graben: Chronological frame. *International Journal of Earth Sciences* **99,** 1955-1974.

Fruergaard, M., Andersen, T. J., Nielsen, L. H., Madsen, A. T., Johannessen, P. N., Murray, A. S., Kirkegaard, L., and Pejrup, M. (2011). Punctuated sediment record resulting from channel migration in a shallow sand-dominated micro-tidal lagoon, Northern Wadden Sea, Denmark. *Marine Geology* **280,** 91-104.

Ganzawa, Y., and Ike, M. (2011). SAR-RTL dating of single grains of volcanic quartz from the late Pleistocene Toya Caldera. *Quaternary Geochronology* **6,** 42-49.

Gillmore, G. K., Stevens, T., Buylaert, J. P., Coningham, R. A. E., Batt, C., Fazeli, H., Young, R., and Maghsoudi, M. (2011). Geoarchaeology and the value of multidisciplinary palaeoenvironmental approaches: a case study from the Tehran Plain, Iran. *Geological Society, London, Special Publications* **352,** 49-67.

Goedicke, C. (2011). Dating mortar by optically stimulated luminescence: A feasibility study. *Geochronometria* **38,** 42-49.

Grove, K., Sklar, L. S., Scherer, A. M., Lee, G., and Davis, J. (2010). Accelerating and spatially-varying crustal uplift and its geomorphic expression, San Andreas Fault zone north of San Francisco, California. *Tectonophysics* **495,** 256-268.

Guralnik, B., Matmon, A., Avni, Y., Porat, N., and Fink, D. (2011). Constraining the evolution of river terraces with integrated OSL and cosmogenic nuclide data. *Quaternary Geochronology* **6,** 22-32.

Gutiérrez, F., Lucha, P., and Galve, J. P. (2010). Reconstructing the geochronological evolution of large landslides by means of the trenching technique in the Yesa Reservoir (Spanish Pyrenees). *Geomorphology* **124,** 124-136.

Haslam, M., Roberts, R. G., Shipton, C., Pal, J. N., Fenwick, J. L., Ditchfield, P., Boivin, N., Dubey, A. K., Gupta, M. C., and Petraglia, M. (2011). Late Acheulean hominins at the Marine Isotope Stage 6/5e transition in north-central India. *Quaternary Research* **75,** 670-682.

He, Z., Huang, C. C., Zheng, H. B., Zhou, J., Pang, J. L., Li, X. Y., and Wang, L. J. (2011). Holocene loess and its deposition dynamics in the upper reaches of the Huaihe River. *Journal of Geographical Sciences* **21,** 561-573.

Hebenstreit, R., Ivy-Ochs, S., Kubik, P. W., Schlüchter, C., and Böse, M. (2011). Lateglacial and early Holocene surface exposure ages of glacial boulders in the Taiwanese high mountain range. *Quaternary Science Reviews* **30,**

298-311.

Huang, C. C., Pang, J., Zha, X., Su, H., and Jia, Y. (2011). Extraordinary floods related to the climatic event at 4200 a BP on the Qishuihe River, middle reaches of the Yellow River, China. *Quaternary Science Reviews* **30,** 460-468.

Huntley, D. J. (2011). Comment on "Isochron dating of sediments using luminescence of K-feldspar grains" by B. Li et al. *J. Geophys. Res.* **116,** F01012.

Huntley, D. J. (2011). Comment on "Isochron measurements of naturally irradiated K-feldspar grains" by B. Li, S.-H. Li, A.G. Wintle and H. Zhao. Radiation Measurements 42, 1315-1327, 2007. *Radiation Measurements* **46,** 166-167.

Jain, M., and Ankjærgaard, C. (2011). Towards a non-fading signal in feldspar: Insight into charge transport and tunnelling from time-resolved optically stimulated luminescence. *Radiation Measurements* **46,** 292-309.

Jiang, H., Mao, X., Xu, H., Thompson, J., Wang, P., and Ma, X. (2011). Last glacial pollen record from Lanzhou (Northwestern China) and possible forcing mechanisms for the MIS 3 climate change in Middle to East Asia. *Quaternary Science Reviews* **30,** 769-781.

Joannes-Boyau, R., and Grün, R. (2011). A comprehensive model for CO2- radicals in fossil tooth enamel: Implications for ESR dating. *Quaternary Geochronology* **6,** 82-97.

Juyal, N., Sundriyal, Y., Rana, N., Chaudhary, S., and Singhvi, A. K. (2010). Late Quaternary fluvial aggradation and incision in the monsoon-dominated Alaknanda valley, Central Himalaya, Uttrakhand, India. *Journal of Quaternary Science* **25,** 1293-1304.

Kale, V., Achyuthan, H., Jaiswal, M., and Sengupta, S. (2010). Palaeoflood records from Upper Kaveri River, southern India: Evidence for discrete floods during Holocene. *Geochronometria* **37,** 49-55.

Karimi, A., Frechen, M., Khademi, H., Kehl, M., and Jalalian, A. (2011). Chronostratigraphy of loess deposits in northeast Iran. *Quaternary International* **234,** 124-132.

Khasswneh, S., al-Muheisen, Z., and Abd-Allah, R. (2011). Thermoluminescence dating of pottery objects from Tell Al-Husn, northern Jordan. *Mediterranean Archaeology & Archaeometry* **11,** 41-49.

Kim, M. J., Choi, J. H., and Hong, D. G. (2011). Optically stimulated luminescence and radiocarbon dating of samples from two Palaeolithic sites (Hahwagye-ri and Hwadae-ri) in the middle part of Korean Peninsula. *Geosciences Journal* **15,** 65-70.

King, G. E., Finch, A. A., Robinson, R. A. J., and Hole, D. E. (2011). The problem of dating quartz 1: Spectroscopic ionoluminescence of dose dependence. *Radiation Measurements* **46,** 1-9.

Kitis, G. (2011). A simple method to record thermoluminescence glow-curves between 77 and 300 K. *Nuclear Instruments and Methods in Physics Research Section A: Accelerators, Spectrometers, Detectors and Associated Equipment* **637,** 88-94.

Kook, M. H., Murray, A. S., Lapp, T., Denby, P. H., Ankjærgaard, C., Thomsen, K., Jain, M., Choi, J. H., and Kim, G. H. (2011). A portable luminescence dating instrument. *Nuclear Instruments and Methods in Physics Research Section B: Beam Interactions with Materials and Atoms* **269,** 1370-1378.

Kundu, H., Thakkar, M., Biswas, R., and Singhvi, A. (2010). Optical dating of sediments in Khari River basin and slip rate along Katrol Hill Fault (KHF), Kachchh, India. *Geochronometria* **37,** 21-28.

Kunz, A., Frechen, M., Ramesh, R., and Urban, B. (2010). Revealing the coastal event-history of the Andaman Islands (Bay of Bengal) during the Holocene using radiocarbon and OSL dating. *International Journal of Earth Sciences* **99,** 1741-1761.

Lauer, T., Krbetschek, M., Frechen, M., Tsukamoto, S., Hoselmann, C., and Weidenfeller, M. (2011). Infrared radiofluorescence (IR-RF) dating of middle pleistocene fluvial archives of the Heidelberg Basin (Southwest Germany). *Geochronometria* **38,** 23-33.

Lauer, T., Frechen, M., Klostermann, J., Krbetschek, M., Schollmayer, G., and Tsukamoto, S. (2011). Luminescence dating of Last Glacial and Early Holocene fluvial deposits from the Lower Rhine methodological aspects and chronological framework. *Zeitschrift der Deutschen Gesellschaft für Geowissenschaften* **162,** 47-61.

Lee, M. K., Lee, Y. I., Lim, H. S., Lee, J. I., Choi, J. H., and Yoon, H. I. (2011). Comparison of radiocarbon and OSL dating methods for a Late Quaternary sediment core from Lake Ulaan, Mongolia. *Journal of Paleolimnology* **45,** 127-135.

Lepper, K., Crowell, K., and Wilson, C. (2011). Chronology of colluvial apron deposition within Cañada del Buey, Pajarito Plateau, New Mexico. *New Mexico Geology* **33,** 3-8.

Li, B., and Li, S.-H. (2011). Thermal stability of infrared stimulated luminescence of sedimentary K-feldspar. *Radiation Measurements* **46,** 29-36.

Li, B., Li, S. H., and Zhao, H. (2011). Reply to comment by Huntley on "isochron dating of sediments using luminescence of K-feldspar grains". *Journal of Geophysical Research F: Earth Surface* **116**.

Li, B., Li, S.-H., Duller, G. A. T., and Wintle, A. G. (2011). Infrared stimulated luminescence measurements of single grains of K-rich feldspar for isochron dating. *Quaternary Geochronology* **6,** 71-81.

Li, B., Li, S.-H., Wintle, A. G., and Zhao, H. (2011). Anomalous fading: A reply to the comment by Huntley on "Isochron measurements of naturally irradiated K-feldspar grains". *Radiation Measurements* **46,** 164-165.

Li, G.-Q., Zhao, H., and Chen, F.-H. (2011). Comparison of three K-feldspar luminescence dating methods for Holocene samples. *Geochronometria* **38,** 14-22.

Liritzis, I., Polymeris, G. S., and Zacharias, N. (2010). Surface luminescence dating of 'Dragon Houses' and Armena Gate at Styra (Euboea, Greece). *Mediterranean Archaeology & Archaeometry* **10,** 65-81.

Little, T. A., Van Dissen, R., Rieser, U., Smith, E. G. C., and Langridge, R. M. (2010). Coseismic strike slip at a point during the last four earthquakes on the Wellington fault near Wellington, New Zealand. *Journal of Geophysical Research B: Solid Earth* **115,** B05403.

Liu, J., Saito, Y., Kong, X., Wang, H., Wen, C., Yang, Z., and Nakashima, R. (2010). Delta development and channel incision during marine isotope stages 3 and 2 in the western South Yellow Sea. *Marine Geology* **278,** 54-76.

Liu, J. F., Chen, J., Yin, J. H., Lu, Y. C., Murray, A., Chen, L. C., Thompson, J., and Yang, H. L. (2010). OSL and AMS ^{14}C dating of the penultimate earthquake at the leigu trench along the Beichuan fault, Longmen Shan, in the northeast margin of the Tibetan plateau. *Bulletin of the Seismological Society of America* **100,** 2681-2688.

Liu, X., Lai, Z., Madsen, D., Yu, L., Liu, K., and Zhang, J. (2011). Lake level variations of Qinghai Lake in northeastern Qinghai-Tibetan Plateau since 3.7 ka based on OSL dating. *Quaternary International* **236,** 57-64.

Lomax, J., Hilgers, A., and Radtke, U. (2011). Palaeoenvironmental change recorded in the palaeodunefields of the western Murray Basin, South Australia - New data from single grain OSL-dating. *Quaternary Science Reviews* **30,**

723-736.

Long, H., Lai, Z., Wang, N., and Zhang, J. (2011). A combined luminescence and radiocarbon dating study of Holocene lacustrine sediments from arid northern China. *Quaternary Geochronology* **6,** 1-9.

Lowick, S. E., and Preusser, F. (2011). Investigating age underestimation in the high dose region of optically stimulated luminescence using fine grain quartz. *Quaternary Geochronology* **6,** 33-41.

Lu, H., Sun, X., Wang, S., Cosgrove, R., Zhang, H., Yi, S., Ma, X., Wei, M., and Yang, Z. (2011). Ages for hominin occupation in Lushi Basin, middle of South Luo River, central China. *Journal of Human Evolution* **60,** 612-617.

Lu, H., Zhao, C., Mason, J., Yi, S., Zhao, H., Zhou, Y., Ji, J., Swinehart, J., and Wang, C. (2011). Holocene climatic changes revealed by aeolian deposits from the Qinghai Lake area (northeastern Qinghai-Tibetan Plateau) and possible forcing mechanisms. *The Holocene* **21,** 297-304.

Madritsch, H., Preusser, F., Fabbri, O., Bichet, V., Schlunegger, F., and Schmid, S. M. (2010). Late Quaternary folding in the Jura Mountains: evidence from syn-erosional deformation of fluvial meanders. *Terra Nova* **22,** 147-154.

Madsen, A. T., Murray, A. S., Andersen, T. J., and Pejrup, M. (2010). Luminescence dating of Holocene sedimentary deposits on Rømø, a barrier island in the Wadden Sea, Denmark. *The Holocene* **20,** 1247-1256.

Madsen, A. T., Murray, A. S., Jain, M., Andersen, T. J., and Pejrup, M. (2011). A new method for measuring bioturbation rates in sandy tidal flat sediments based on luminescence dating. *Estuarine, Coastal and Shelf Science* **92,** 464-471.

Mauz, B., Baeteman, C., Bungenstock, F., and Plater, A. J. (2010). Optical dating of tidal sediments: Potentials and limits inferred from the North Sea coast. *Quaternary Geochronology* **5,** 667-678.

Mikulcic Pavlakovic, S., Crnjakovic, M., Tibljas, D., Soufek, M., Wacha, L., Frechen, M., and Lackovic, D. (2011). Mineralogical and geochemical characteristics of Quaternary sediments from the Island of Susak (Northern Adriatic, Croatia). *Quaternary International* **234,** 32-49.

Morin, E., Macaire, J.-J., Hinschberger, F., Gay-Ovéjéro, I., Rodrigues, S., Bakyono, J.-P., and Visset, L. (2011). Spatio-temporal evolution of the Choisille River (southern Parisian Basin, France) during the Weichselian and the Holocene as a record of climate trend and human activity in north-western Europe. *Quaternary Science Reviews* **30,** 347-363.

Moska, P., Adamiec, G., and Jary, Z. (2011). OSL dating and lithological characteristics of loess deposits from Biały Kościół. *Geochronometria* **38,** 162-171.

Moura-Lima, E. N., Bezerra, F. H. R., Lima-Filho, F. P., de Castro, D. L., Sousa, M. O. L., Fonseca, V. P., and Aquino, M. R. (2011). 3-D geometry and luminescence chronology of Quaternary soft-sediment deformation structures in gravels, northeastern Brazil. *Sedimentary Geology* **235,** 160-171.

Muñoz-Salinas, E., Bishop, P., Sanderson, D. C. W., and Zamorano, J.-J. (2011). Interpreting luminescence data from a portable OSL reader: three case studies in fluvial settings. *Earth Surface Processes and Landforms* **36,** 651-660.

Munyikwa, K., Feathers, J. K., Rittenour, T. M., and Shrimpton, H. K. (2011). Constraining the Late Wisconsinan retreat of the Laurentide ice sheet from western Canada using luminescence ages from postglacial aeolian dunes. *Quaternary Geochronology* **6,** 407-422.

Nádor, A., Sinha, R., Magyari, Á., Tandon, S. K., Medzihradszky, Z., Babinszki, E., Thamó-Bozsó, E., Unger, Z., and Singh, A. (2011). Late Quaternary (Weichselian) alluvial history and neotectonic control on fluvial landscape development in the southern Körös plain, Hungary. *Palaeogeography, Palaeoclimatology, Palaeoecology* **299,** 1-14.

Nelson, N. A., and Pierce, J. (2010). Late-Holocene relationships among fire, climate and vegetation in a forest-sagebrush ecotone of southwestern Idaho, USA. *The Holocene* **20,** 1179-1194.

Notebaert, B., Verstraeten, G., Vandenberghe, D., Marinova, E., Poesen, J., and Govers, G. (2011). Changing hillslope and fluvial Holocene sediment dynamics in a Belgian loess catchment. *Journal of Quaternary Science* **26,** 44-58.

Novothny, Á., Frechen, M., Horváth, E., Wacha, L., and Rolf, C. (2011). Investigating the penultimate and last glacial cycles of the Sütto loess section (Hungary) using luminescence dating, high-resolution grain size, and magnetic susceptibility data. *Quaternary International* **234,** 75-85.

Okumura, T., Toyoda, S., Sato, F., Uchida, A., Ishibashi, J.-I., and Nakai, S. i. (2010). ESR dating of marine barite in chimneys deposited from hydrothermal vents. *Geochronometria* **37,** 57-61.

Owen, L. A., Frankel, K. L., Knott, J. R., Reynhout, S., Finkel, R. C., Dolan, J. F., and Lee, J. (2011). Beryllium-10 terrestrial cosmogenic nuclide surface exposure dating of Quaternary landforms in Death Valley. *Geomorphology* **125,** 541-557.

Pagonis, V., Adamiec, G., Athanassas, C., Chen, R., Baker, A., Larsen, M., and Thompson, Z. (2011). Simulations of thermally transferred OSL signals in quartz: Accuracy and precision of the protocols for equivalent dose evaluation. *Nuclear Instruments and Methods in Physics Research Section B: Beam Interactions with Materials and Atoms* **269,** 1431-1443.

Pagonis, V., Baker, A., Larsen, M., and Thompson, Z. (2011). Precision and accuracy of two luminescence dating techniques for retrospective dosimetry: SAR-OSL and SAR-ITL. *Nuclear Instruments and Methods in Physics Research Section B: Beam Interactions with Materials and Atoms* **269,** 653-663.

Pagonis, V., Chen, R., and Kitis, G. (2011). On the intrinsic accuracy and precision of luminescence dating techniques for fired ceramics. *Journal of Archaeological Science* **38,** 1591-1602.

Pánek, T., Táborík, P., Klimes, J., Komárková, V., Hradecký, J., and Stastný, M. (2011). Deep-seated gravitational slope deformations in the highest parts of the Czech Flysch Carpathians: Evolutionary model based on kinematic analysis, electrical imaging and trenching. *Geomorphology* **129,** 92-112.

Pati, P., Parkash, B., Awasthi, A. K., and Acharya, V. (2011). Holocene tectono-geomorphic evolution of parts of the Upper and Middle Gangetic plains, India. *Geomorphology* **128,** 148-170.

Pedersen, J. B. T., Jakobsen, B. H., and Kroon, A. (2010). Optically Stimulated Luminescence dating of Inuit settlement structures in coastal landscapes of Northeast Greenland. *Geografisk Tidsskrift* **110,** 365-371.

Pierce, J. L., Meyer, G. A., and Rittenour, T. (2011). The relation of Holocene fluvial terraces to changes in climate and sediment supply, South Fork Payette River, Idaho. *Quaternary Science Reviews* **30,** 628-645.

Preusser, F., Schmitt, L., Delile, H., and Grosprêtre, L. (2011). Optically stimulated luminescence (OSL) dating of the sedimentation history of the Yzeron Basin (Chaudanne sub-catchment), Rhône valley, France. *Quaternaire* **22,** 73-83.

Price, G. J., Webb, G. E., Zhao, J.-X., Feng, Y.-X., Murray, A. S., Cooke, B. N., Hocknull, S. A., and Sobbe, I. H. (2011). Dating megafaunal extinction on the Pleistocene Darling Downs, eastern Australia: the promise and pitfalls

of dating as a test of extinction hypotheses. *Quaternary Science Reviews* **30,** 899-914.

Prideaux, G. J., Gully, G. A., Couzens, A. M. C., Ayliffe, L. K., Jankowski, N. R., Jacobs, Z., Roberts, R. G., Hellstrom, J. C., Gagan, M. K., and Hatcher, L. M. (2010). Timing and dynamics of Late Pleistocene mammal extinctions in southwestern Australia. *Proceedings of the National Academy of Sciences* **107,** 22157-22162.

Quang-Minh, D., Frechen, M., Nghi, T., and Harff, J. (2010). Timing of Holocene sand accumulation along the coast of central and SE Vietnam. *International Journal of Earth Sciences* **99,** 1731-1740.

Raukas, A., Stankowski, W., Zelčs, V., and Šinkunas, P. (2010). Chronology of the Last Deglaciation in the southeastern Baltic region on the basis of recent OSL dates. *Geochronometria* **36,** 47-54.

Reimann, T., Tsukamoto, S., Naumann, M., and Frechen, M. (2011). The potential of using K-rich feldspars for optical dating of young coastal sediments - A test case from Darss-Zingst peninsula (southern Baltic Sea coast). *Quaternary Geochronology* **6,** 207-222.

Ren, J., Chen, G., Xu, X., Zhang, S., and Mao, C. (2010). Surface rupture of the 2008 Wenchuan, China, earthquake in the qingping stepover determined from geomorphologic surveying and excavation, and its tectonic implications. *Bulletin of the Seismological Society of America* **100,** 2651-2659.

Rich, J., and Stokes, S. (2011). A 200,000-year record of late Quaternary aeolian sedimentation on the Southern High Plains and nearby Pecos River Valley, USA. *Aeolian Research* **2,** 221-240.

Rizza, M., Mahan, S., Ritz, J. F., Nazari, H., Hollingsworth, J., and Salamati, R. (2011). Using luminescence dating of coarse matrix material to estimate the slip rate of the Astaneh fault, Iran. *Quaternary Geochronology* **6,** 390-406.

Rossetti, D. F., Bezerra, F. H. R., Goes, A. M., Valeriano, M. M., Andrades-Filho, C. O., Mittani, J. C. R., Tatumi, S. H., and Brito-Neves, B. B. (2011). Late Quaternary sedimentation in the Paraiba Basin, Northeastern Brazil: Landform, sea level and tectonics in Eastern South America passive margin. *Palaeogeography Palaeoclimatology Palaeoecology* **300,** 191-204.

Saini, H., and Mujtaba, S. (2010). Luminescence dating of the sediments from a buried channel loop in Fatehabad area, Haryana: Insight into Vedic Saraswati River and its environment. *Geochronometria* **37,** 29-35.

Sallun, A. E. M., and Suguio, K. (2010). Quaternary colluvial episodes (Upper Paraná River Hydrographic Basin, Brazil). *Anais da Academia Brasileira de Ciencias* **82,** 701-715.

Santana, S. T., Khoury, H. J., Sullasi, H. L., and Guzzo, P. L. (2010). Luminescence properties of feldspars from the Northeast region of Brazil. *Journal of Physics: Conference Series* **249**.

Sawakuchi, A. O., Blair, M. W., DeWitt, R., Faleiros, F. M., Hyppolito, T., and Guedes, C. C. F. (2011). Thermal history versus sedimentary history: OSL sensitivity of quartz grains extracted from rocks and sediments. *Quaternary Geochronology* **6,** 261-272.

Schirrmeister, L., Grosse, G., Schnelle, M., Fuchs, M., Krbetschek, M., Ulrich, M., Kunitsky, V., Grigoriev, M., Andreev, A., Kienast, F., Meyer, H., Babiy, O., Klimova, I., Bobrov, A., Wetterich, S., and Schwamborn, G. (2011). Late Quaternary paleoenvironmental records from the western Lena Delta, Arctic Siberia. *Palaeogeography, Palaeoclimatology, Palaeoecology* **299,** 175-196.

Schmidt, A., Quigley, M., Fattahi, M., Azizi, G., Maghsoudi, M., and Fazeli, H. (2011). Holocene settlement shifts and palaeoenvironments on the Central Iranian Plateau: Investigating linked systems. *The Holocene* **21,** 583-595.

Schmidt, E. D., Frechen, M., Murray, A. S., Tsukamoto, S., and Bittmann, F. (2011). Luminescence chronology of

the loess record from the Tönchesberg section: A comparison of using quartz and feldspar as dosimeter to extend the age range beyond the Eemian. *Quaternary International* **234,** 10-22.

Schütt, B., Frechen, M., Hoelzmann, P., and Fritzenwenger, G. (2011). Late Quaternary landscape evolution in a small catchment on the Chinese Loess Plateau. *Quaternary International* **234,** 159-166.

Seong, Y. B., Kang, H.-C., Ree, J.-H., Choi, J.-H., Lai, Z., Long, H., and Yoon, H. O. (2011). Geomorphic constraints on active mountain growth by the lateral propagation of fault-related folding: A case study on Yumu Shan, NE Tibet. *Journal of Asian Earth Sciences* **41,** 184-194.

Shaanan, U., Porat, N., Navon, O., Weinberger, R., Calvert, A., and Weinstein, Y. (2011). OSL dating of a Pleistocene maar: Birket Ram, the Golan heights. *Journal of Volcanology and Geothermal Research* **201,** 397-403.

Sier, M. J., Roebroeks, W., Bakels, C. C., Dekkers, M. J., Brühl, E., De Loecker, D., Gaudzinski-Windheuser, S., Hesse, N., Jagich, A., Kindler, L., Kuijper, W. J., Laurat, T., Mücher, H. J., Penkman, K. E. H., Richter, D., and van Hinsbergen, D. J. J. (2011). Direct terrestrial-marine correlation demonstrates surprisingly late onset of the last interglacial in central Europe. *Quaternary Research* **75,** 213-218.

Simms, A. R., DeWitt, R., Kouremenos, P., and Drewry, A. M. (2011). A new approach to reconstructing sea levels in Antarctica using optically stimulated luminescence of cobble surfaces. *Quaternary Geochronology* **6,** 50-60.

Singh, L. L., and Gartia, R. K. (2011). A new method of determination of trapping parameters of glow peaks relevant to dosimetry and dating from their lifetime. *Radiation Effects and Defects in Solids* **166,** 297-304.

Singhvi, A. K., Williams, M. A. J., Rajaguru, S. N., Misra, V. N., Chawla, S., Stokes, S., Chauhan, N., Francis, T., Ganjoo, R. K., and Humphreys, G. S. (2010). A ~200 ka record of climatic change and dune activity in the Thar Desert, India. *Quaternary Science Reviews* **29,** 3095-3105.

Slimak, L., Svendsen, J. I., Mangerud, J., Plisson, H., Heggen, H. P., Brugère, A., and Pavlov, P. Y. (2011). Late Mousterian Persistence near the Arctic Circle. *Science* **332,** 841-845.

Soares, E. A. A., Tatumi, S. H., and Riccomini, C. (2010). OSL age determinations of Pleistocene fluvial deposits in Central Amazonia. *Anais da Academia Brasileira de Ciencias* **82,** 691-699.

Stankowski, W. (2011). Luminescence and radiocarbon dating as tools for the recognition of extraterrestrial impacts. *Geochronometria* **38,** 50-54.

Steffen, D., Schlunegger, F., and Preusser, F. (2010). Late Pleistocene fans and terraces in the Majes valley, southern Peru, and their relation to climatic variations. *International Journal of Earth Sciences* **99,** 1975-1989.

Stevens, T., Markovic, S. B., Zech, M., Hambach, U., and Sümegi, P. (2011). Dust deposition and climate in the Carpathian Basin over an independently dated last glacial-interglacial cycle. *Quaternary Science Reviews* **30,** 662-681.

Strahl, J., Krbetschek, M. R., Luckert, J., Machalett, B., Meng, S., Oches, E. A., Ivo Rappsilber, Wansa, S., and Zöller, L. (2011). Geologie, Paläontologie und Geochronologie des Eem-Beckens Neumark-Nord 2 und Vergleich mit dem Becken Neumark-Nord 1 (Geiseltal, Sachsen-Anhalt). *E&G Quaternary Science Journal* **59,** 120–167.

Subedi, B., Oniya, E., Polymeris, G. S., Afouxenidis, D., Tsirliganis, N. C., and Kitis, G. (2011). Thermal quenching of thermoluminescence in quartz samples of various origin. *Nuclear Instruments and Methods in Physics Research Section B: Beam Interactions with Materials and Atoms* **269,** 572-581.

Svendsen, J. I., Heggen, H. P., Hufthammer, A. K., Mangerud, J., Pavlov, P., and Roebroeks, W. (2010). Geo-

archaeological investigations of Palaeolithic sites along the Ural Mountains - On the northern presence of humans during the last Ice Age. *Quaternary Science Reviews* **29,** 3138-3156.

Tan, Z., Huang, C. C., Pang, J., and Zhou, Q. (2011). Holocene wildfires related to climate and land-use change over the Weihe River Basin, China. *Quaternary International* **234,** 167-173.

Tatumi, S. H., Bitencourt, J. F. S., de Silva, D. M., Lyra, J. S., Kinoshita, A., and Sullasi, H. S. L. (2010). Study of the effects of heat treatments in the paramagnetic centers of alkaline feldspars and their implications in the luminescence properties. *Journal of Physics: Conference Series* **249,** 012026.

Thiel, C., Buylaert, J.-P., Murray, A., Terhorst, B., Hofer, I., Tsukamoto, S., and Frechen, M. (2011). Luminescence dating of the Stratzing loess profile (Austria) - Testing the potential of an elevated temperature post-IR IRSL protocol. *Quaternary International* **234,** 23-31.

Thomsen, K., Murray, A., and Jain, M. (2011). Stability of IRSL signals from sedimentary K-feldspar samples. *Geochronometria* **38,** 1-13.

Timmons, E. A., Rodriguez, A. B., Mattheus, C. R., and DeWitt, R. (2010). Transition of a regressive to a transgressive barrier island due to back-barrier erosion, increased storminess, and low sediment supply: Bogue Banks, North Carolina, USA. *Marine Geology* **278,** 100-114.

Tokuyasu, K., Tanaka, K., Tsukamoto, S., and Murray, A. (2010). The characteristics of OSL signal from quartz grains extracted from modern sediments in Japan. *Geochronometria* **37,** 13-19.

Tolksdorf, J. F., Kaiser, K., Terberger, T., Klasen, N., Schneider, B., and Masberg, P. (2011). Aeolian sedimentation in the Rhine and Main area from the Late Glacial until the Mid-Holocene. *E&G Quaternary Science Journal* **59,** 36–43.

Tsukamoto, S., Duller, G. A. T., Wintle, A. G., and Muhs, D. (2011). Assessing the potential for luminescence dating of basalts. *Quaternary Geochronology* **6,** 61-70.

Tsukamoto, S., Nagashima, K., Murray, A. S., and Tada, R. (2011). Variations in OSL components from quartz from Japan sea sediments and the possibility of reconstructing provenance. *Quaternary International* **234,** 182-189.

Van Mourik, J. M., Slotboom, R. T., and Wallinga, J. (2011). Chronology of plaggic deposits; palynology, radiocarbon and optically stimulated luminescence dating of the Posteles (NE-Netherlands). *Catena* **84,** 54-60.

Vasiliniuc, Ş., Timar-Gabor, A., Vandenberghe, D. A. G., Panaiotu, C. G., Begy, R., and Cosma, C. (2011). A high resolution optical dating study of the Mostiştea loess-palaeosol sequence (SE Romania) using sand-sized quartz. *Geochronometria* **38,** 34-41-41.

Vincent, P. J., Lord, T. C., Telfer, M. W., and Wilson, P. (2011). Early Holocene loessic colluviation in northwest England: new evidence for the 8.2 ka event in the terrestrial record? *Boreas* **40,** 105-115.

Vogelsang, R., Richter, J., Jacobs, Z., Eichhorn, B., Linseele, V., and Roberts, R. G. (2010). New Excavations of Middle Stone Age Deposits at Apollo 11 Rockshelter, Namibia: Stratigraphy, Archaeology, Chronology and Past Environments. *Journal of African Archaeology* **8**.

Wacha, L., Mikulcic Pavlakovic, S., Novothny, Á., Crnjakovic, M., and Frechen, M. (2011). Luminescence dating of Upper Pleistocene loess from the Island of Susak in Croatia. *Quaternary International* **234,** 50-61.

Walker, R. T., Claisse, S., Telfer, M., Nissen, E., England, P., Bryant, C., and Bailey, R. (2010). Preliminary estimate of Holocene slip rate on active normal faults bounding the southern coast of the Gulf of Evia, central

Greece. *Geosphere* **6,** 583-593.

Wang, P., Zhang, B., Qiu, W., and Wang, J. (2011). Soft-sediment deformation structures from the Diexi paleo-dammed lakes in the upper reaches of the Minjiang River, east Tibet. *Journal of Asian Earth Sciences* **40,** 865-872.

Waters, M. R., Forman, S. L., Jennings, T. A., Nordt, L. C., Driese, S. G., Feinberg, J. M., Keene, J. L., Halligan, J., Lindquist, A., Pierson, J., Hallmark, C. T., Collins, M. B., and Wiederhold, J. E. (2011). The Buttermilk Creek Complex and the Origins of Clovis at the Debra L. Friedkin Site, Texas. *Science* **331,** 1599-1603.

Weiguo Liu, Zhonghui Liu, Zhisheng An, Xulong Wang, and Hong Chang. (2011). Wet climate during the 'Little Ice Age' in the arid Tarim Basin, northwestern China. *The Holocene* **21,** 409-416.

Wenban-Smith, F. F., Bates, M. R., and Schwenninger, J.-L. (2010). Early Devensian (MIS 5d–5b) occupation at Dartford, southeast England. *Journal of Quaternary Science* **25,** 1193-1199.

Wenske, D., Böse, M., Frechen, M., and Lüthgens, C. (2011). Late Holocene mobilisation of loess-like sediments in Hohuan Shan, high mountains of Taiwan. *Quaternary International* **234,** 174-181.

Wintle, A. (2010). Future Directions of Luminescence Dating of Quartz. *Geochronometria* **37,** 1-7.

Woda, C., Ulanovsky, A., Bougrov, N. G., Fiedler, I., Degteva, M. O., and Jacob, P. (2011). Potential and limitations of the 210 °C TL peak in quartz for retrospective dosimetry. *Radiation Measurements* **46,** 485-493.

Wohlfarth, B., Alexanderson, H., Ampel, L., Bennike, O. L. E., Engels, S., Johnsen, T., Lundqvist, J. A. N., and Reimer, P. (2011). Pilgrimstad revisited – a multi-proxy reconstruction of Early/Middle Weichselian climate and environment at a key site in central Sweden. *Boreas* **40,** 211-230.

Wolfe, S., Bond, J., and Lamothe, M. (2011). Dune stabilization in central and southern Yukon in relation to early Holocene environmental change, northwestern North America. *Quaternary Science Reviews* **30,** 324-334.

Yamamoto, Y., Toyoda, S., Nagasima, K., Igarashi, Y., and Tada, R. (2010). The Grain Size Influence on the E1' Centre Observed in Quartz of Atmospheric Deposition at Two Japanese Cities: A Preliminary Study. *Geochronometria* **37,** 9-12.

Yang, G., Zhang, X., Tian, M., Brierley, G., Chen, A., Ping, Y., Ge, Z., Ni, Z., and Yang, Z. (2011). Alluvial terrace systems in Zhangjiajie of northwest Hunan, China: Implications for climatic change, tectonic uplift and geomorphic evolution. *Quaternary International* **233,** 27-39.

Yin, G., Bahain, J.-J., Shen, G., Tissoux, H., Falguères, C., Dolo, J.-M., Han, F., and Shao, Q. (2011). ESR/U-series study of teeth recovered from the palaeoanthropological stratum of the Dali Man site (Shaanxi Province, China). *Quaternary Geochronology* **6,** 98-105.

Zhang, J.-F., Wang, X.-Q., Qiu, W.-L., Shelach, G., Hu, G., Fu, X., Zhuang, M.-G., and Zhou, L.-P. (2011). The paleolithic site of Longwangchan in the middle Yellow River, China: chronology, paleoenvironment and implications. *Journal of Archaeological Science* **38,** 1537-1550.

Zieliński, P., Sokołowski, R., Fedorowicz, S., and Jankowski, M. (2011). Stratigraphic position of fluvial and aeolian deposits in the Żabinko site (W Poland) based on TL dating. *Geochronometria* **38,** 64-71.

Zöller, L., Hambach, U., Blanchard, H., Fischer, S., Köhne, S., and Stritzke, R. (2011). Der Rodderberg-Krater bei Bonn. *E&G Quaternary Science Journal* **59,** 44–58.

Letters

_____

Some comments arising from Berger (2010)

R. F. Galbraith

Department of Statistical Science, University College London, Gower Street, London, WC1E 6BT, UK (e-mail: rex@stats.ucl.ac.uk)

Abstract

I note a fundamental error in the "alternate form of probability-distribution plot" proposed by Berger (2010a) and comment on some related issues, including transformations, radial plots, empirical distributions, kernel density estimates, weighted means and selected data.

Introduction

In a recent article in this journal (Galbraith 2010) I discussed, among other things, a type of "probability density" graph that has sometimes been used to display OSL equivalent doses for a sample of single grains or aliquots. In this graph, each D_e value is replaced by a Gaussian curve centered on the observed D_e with standard deviation equal to the standard error of D_e and the curves are then summed pointwise. I referred to this specifically as a "PD" graph and distinguished it from a conventional kernel density estimate (KDE). I tried to explain what it is doing and why it is not to be recommended.

Also, and perhaps more importantly, I tried to encourage researchers to think about the *meaning* of an equivalent dose frequency distribution. To what extent does it represent frequencies in a natural population, rather than artefacts of sampling and grain selection or variation in luminescence and experimental procedures? I also distinguished between the distributions of *true* equivalent doses (where hypothetically, D_e values are measured without error) and *observed* D_e values, a distinction necessary for understanding data and making reliable inferences.

In the same issue of this journal, Berger (2010a) proposed an "alternate form of probability-distribution plot" for OSL equivalent doses, which he called a "Transformed-PD" plot, or TPD plot for short. The essence of this was to construct the sum of Gaussian curves using log D_e values and relative standard errors, rather than actual D_e values and their absolute standard errors. But the probability density curves so obtained were presented on a linear D_e scale, having apparently been transformed (without comment) from the log D_e scale. Unfortunately this transformation was not done correctly and they do not represent the intended probability distributions — and they do not have the meaning attributed to them in that paper, as acknowledged by Berger (2010b).

Berger (2010a) also presented some interesting data examples and raised several other issues that are perhaps worth further comment — concerning radial plots, log transformations, empirical distributions, kernel density estimates, weighted means and selected data. He rightly noted that radial plots offer advantages over PD plots. In fact his radial plots are far more informative than his corresponding PD and empirical distribution plots, and his data presentation would be less convincing without them. This is not to say that one should make *only* radial plots of D_e values, but it supports my recommendation to look at them in addition to other plots that might be made. Berger (2010a) also stated that radial plots could not be used for samples containing zero or negative D_e values, because they use a logarithmic transformation. But of course one can make a radial plot without using a log transformation (or indeed any transformation), as acknowledged by Berger (2010b).

However, what Berger (2010a, page 13) saw as the "two main criticisms" of the conventional PD plot are merely to do with the nature of the empirical distributions of D_e values and their errors, and he did not recognise the more fundamental problems noted in Galbraith (1998) and Galbraith (2010). These are to do with their meaning and interpretation. On one level, a PD plot might just be regarded as an empirical smoothing of the data. If so, it is a poor one compared with, say, a conventional KDE where the kernel bandwidth is chosen according to sample size (among other things). But often PD plots are mis-interpreted and lead to fallacious arguments and unconvincing science.

I elaborate on some of these points below. This article is not intended to be a comprehensive critique of Berger (2010a) but rather a discussion of some statistical issues arising there and elsewhere in the OSL literature.

Transforming a probability density function

To illustrate the incorrect transformation mentioned above, look at the solid line in Berger (2010a, Figure 3). That curve is supposed to correspond, on the natural log scale, to an equal mixture (or sum) of four Gaussian probability density functions (pdfs) all with the same standard deviation (equal to 0.10) and means log(5), log(10), log(20) and log(30). If we transform this to the linear scale, it can be shown that we should get an equal mixture (or sum) of four *log-normal* pdfs. You can see that the TPD curve drawn must be wrong because the areas under its component curves should be equal and they are not.

When introducing his method, Berger (2010a, page 14) wrote: "However, application of equation 2 to these same artificial data generates the solid curve in Figure 3, accurately representing their respective probabilities". But his equation 2 does not generate the solid curve in his Figure 3, and that figure does not accurately represent their respective probabilities.

Figure 1 shows the correct distribution on both log and linear scales. The top panel shows the pdf of Z (corresponding to log D_e), denoted by $f(z)$, and the bottom panel shows the pdf of W (corresponding to D_e) denoted by $g(w)$, where $Z = \log(W)$. The formula relating these two pdfs is

$$g(w) = f(\log(w)) / w$$

for positive w. The factor $1/w$ is called the Jacobian of the transformation and is required in order to preserve the validity of probability statements, which are related to areas under the curve. That is, the probability that W lies between a and b must equal the probability that $\log(W)$ lies between $\log(a)$ and $\log(b)$ for any a and b. Different transformations have different Jacobians.

The bottom panel of Figure 1 also shows the pdf of a mixture of normal (rather than log-normal) pdfs as a red dotted line. The dashed curve in Berger (2010a, Figure 3) should be the same as this. The red dotted curve can hardly be seen as it differs only very slightly from $g(w)$. This reflects the fact that if a log-normal distribution has a small dispersion then it is very hard to distinguish it from a normal distribution with the same mean and standard deviation. In the present case, each component has a coefficient of variation of 10%, which is small enough to make the normal and log-normal distributions practically the same. If the coefficients of variation were larger then the two curves would differ more.
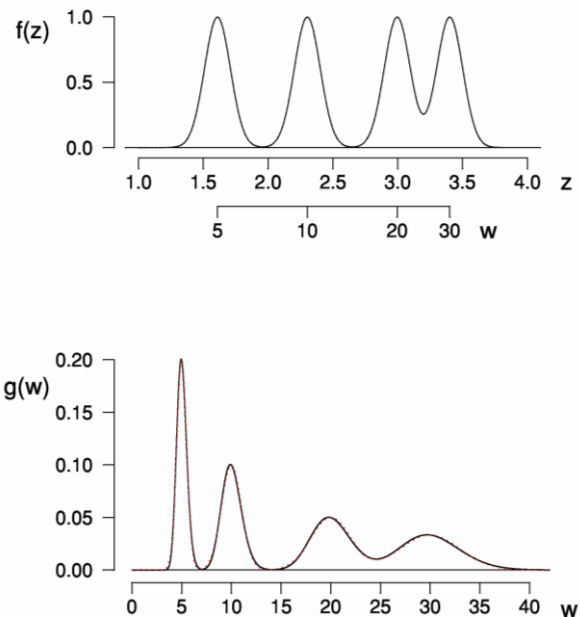

Figure 1: *Upper panel: the pdf f (z) of an equal mixture of four Gaussian pdfs, each with standard deviation 0.10 and means log(5), log(10), log(20) and log(30). Lower panel: the solid curve shows the pdf g(w) of the mixture of log-normal distributions obtained by the transformation w = exp(z) so that z = log(w). The dotted red curve shows an equal mixture of Gaussian pdfs with means 5, 10, 20 and 30, and standard deviations 0.5, 1, 2 and 3, respectively. The w axis corresponds to the scale of D_e and z corresponds to log(D_e).*

This discussion has nothing to do with the merits of PD plots as such, but it is instructive for understanding both log transformations and probability density functions.

What is Berger's TPD plot?

Berger (2010b) confirmed that in drawing his TPD plot on the D_e scale the Jacobian factor was omitted, so that the graph "does not manifest relative probabilities" and he suggested that it shows "rather something more akin to relative 'weighted' frequencies". What is it really a plot of, and is it useful?

Imagine a positive random variable W having a probability density function $g(w)$ describing relative frequencies in a population. Consider plotting a graph of $wg(w)$ against w. The total area under this curve would equal the mean, or expectation, of W; and the area under it between two values a and b would

represent the 'contribution' to the overall mean from values of w in that range. However, it is hard to see what practical use this concept might have. In particular, modes or peaks of $wg(w)$ will not coincide with those of $g(w)$.

Now consider a TPD curve as plotted in Berger (2010a, Figures 3, 4, 6, 8 or 10). Those figures do not have numerical scales on their vertical axes, but it can be shown that the TPD curve is effectively a plot of $wg(w)$ against w, where $g(w)$ is an equal mixture (or sum) of n log-normal pdfs, where n is the number of grains or aliquots in the sample. The ith log-normal pdf in this mixture has mean $y_i \exp(\frac{1}{2} r_i^2)$, where y_i is the observed D_e value for the ith grain and r_i is its relative standard error. The factor multiplying y_i here is slightly greater than 1 and greater for larger r_i. Thus the total area under the TPD curve is the average (or sum) of these means, so is a quantity a bit greater than the un-weighted sample mean (or sum) of observed D_e values. The TPD curve itself would therefore indicate some sort of relative contributions to this quantity from different doses represented in the sample data. The qualification "some sort of" is referring to the rather arbitrary role of the relative standard errors of D_e used in constructing the curve and hence in defining its meaning.

It is clear from this that Berger's TPD plot has no clear-cut interpretation as a frequency distribution of OSL equivalent doses.

Log transformations (or not) in radial plots
A strange idea appears to have arisen that a radial plot must necessarily use a log transformation of D_e and therefore can't be used to represent data containing zero or negative D_e values. Of course it is just as easy to make a radial plot using actual D_e values and their (absolute) standard errors as it is with log D_e values and relative standard errors. Examples of the former can be seen in Arnold et al. (2009) and Galbraith (2010).

Not only is it possible, it is also sometimes *more appropriate* to use a linear D_e scale. For example, when D_e values are close to zero their relative standard errors may happen to be large simply because they are relative to something small, and they may appear to be uninformative on a radial plot that is drawn with respect to relative standard errors, but properly informative when drawn with respect to absolute standard errors. Furthermore, in such cases there may be no clear relationship between D_e values and their standard errors, suggesting that the main sources of error are additive, rather than multiplicative (e.g. Arnold at al., 2009) and hence

that comparisons on the linear D_e scale are more straightforward.

For a radial plot, the choice between using a log or linear D_e scale is partly related to whether points are better compared using relative or absolute standard errors. Another transformation, mentioned in Galbraith (2010), is the modified log transformation $z = \log(w+a)$ for some suitably chosen a. This can be useful to plot data having some large and some zero or negative values. If a is small, the transformation is similar to a log transformation, while if a is large it is more like a linear transformation, so you can think of the value of a as making a compromise between these two extremes.

Why are radial plots more informative?
Radial plots are more informative because they exploit the information in the precisions.

In his Figures 1 and 2 and corresponding text, Berger (2010a) cited a radial plot and "weighted histogram" (PD plot) from Galbraith (1988). These used some artificial data from a discrete two component mixture with component means +0.5 and −0.5. He found it "inexplicable" that I then wrote: "The weighted histogram is superficially attractive and suggests a *bimodal* distribution but does not point to the true *mixture* as informatively as the radial plot does".

Here is an explanation. The radial plot (reproduced as Figure 2 here) shows that the data are completely explained by a discrete two-component mixture — i.e. just two distinct values, roughly equal to +0.5 and −0.5. This is because you can easily imagine two radii going to +0.5 and −0.5 and, by referring to the ±2 scale on the vertical axis, see that *all* of the variation about them can be explained by the observation errors. This happens to be the model that was used to generate the data, but even if we did not know this, it is clear that the data are consistent with it.

Of course, it would be easier to see this by explicitly drawing the two radii with a ±2 shaded band about each. Each point would fall in, or very close to, one or other band. Furthermore their scatter looks like a superposition of homoscedastic random scatter about each line. You can confirm this by drawing your own lines and bands. I did not do this in my paper in order to avoid imposing any specific model and to allow the reader the freedom to consider possible mechanisms that might have produced these data.
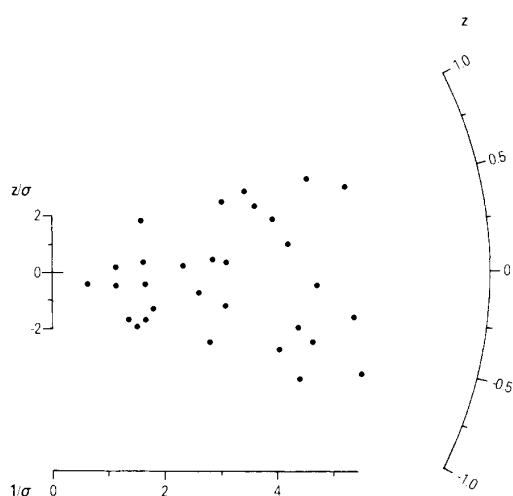
Figure 2: *A radial plot of artificial data from a discrete two component mixture with means +0.5 and −0.5.This is a copy of Figure 2 from Galbraith (1988).*

No such inferences can be made from the PD plot (Galbraith 1988, Figure 9a or Berger 2010a, Figure 2). Although the curve has two modes at about +0.5 and −0.5, it does not tell us either that more than one component is needed to explain the data, or that two is enough. The radial plot tells us both of these things. Furthermore there is no simple relation between the number of components in a mixture distribution and the number of modes its pdf has. For example, it is easy to construct a two component mixture of normal pdfs that is unimodal, and whose mode differs from both component means. Looking at the modes of a PD plot is even more ambiguous because it is not actually estimating the true dose distribution.

In Galbraith (1988, Figure 3) and Berger (2010a, Figure 1) the radial plot is re-drawn with different plotting symbols to show explicitly which observations came from each component. You can see there that most of the low-precision values are consistent with both radii and that many fall closer to the wrong radius (the component that they do not belong to) than to the right one. This reflects uncertainty associated with the observation errors that is inherent in the original data, and that cannot be resolved however you plot them.

That figure is instructive for another reason. Suppose that we wanted to estimate the lowest population component mean value. A method that may naturally spring to mind is to select a subset of points that we think belong to this component and calculate a mean or weighted mean of these. You can see from the

figure that however the subset of points is selected it will always contain some from the higher component or omit some from the lower one. I comment further on this below.

I would encourage those interested to read the whole of that section in my original 1988 paper. That paper also explains the close connection between radial plots and least squares regression though the origin, which helps both with understanding and using radial plots.

Empirical distributions and kernel density estimates
Berger (2010a) rightly pointed out that more information is shown by adding a cumulative plot of ranked data with standard error bars. The individual points show the cumulative empirical distribution of the observed D_e values, and the one-sigma error bars display their standard errors. But a PD plot superimposed on it combines these incorrectly. It would make more sense to draw a conventional kernel density estimate (KDE), or a histogram, in order to see the shape of the distribution of observed D_e values.

The upper panel of Figure 3 shows the ranked observations with one-sigma error bars along with a Gaussian KDE for the data that I used in Galbraith (2010). Here I have chosen the kernel bandwidth to correspond to the bin width in my histogram (Galbraith 2010, Figure 1). The histogram there and KDE here both show the smoothed data to essentially the same degree of resolution. They emphasise slightly different aspects. The KDE shows more detail of the shape of the empirical distribution while the histogram shows numbers of grains and areas under the curve more clearly. The standard errors are displayed in Figure 3, but they are not used in the construction of the KDE.

What bandwidth should one use for a KDE? As with choosing the bin width of a histogram, there is no hard and fast rule. It should depend on the data and purpose. But there are general guidelines in the literature (in the R package, in particular). Note that such guidelines are based on the premise that one is trying to see the shape of the underlying frequency distribution from a sample of observations measured without error, which is usually not the case with observed equivalent doses.

The bandwidth of 0.058 in the upper panel of Figure 2 is very close to the value given by the R function bw.ucv (unbiased cross-validation) applied to these data, which is 0.061. In the lower panel I have drawn the graph again but using the bandwidth given by the
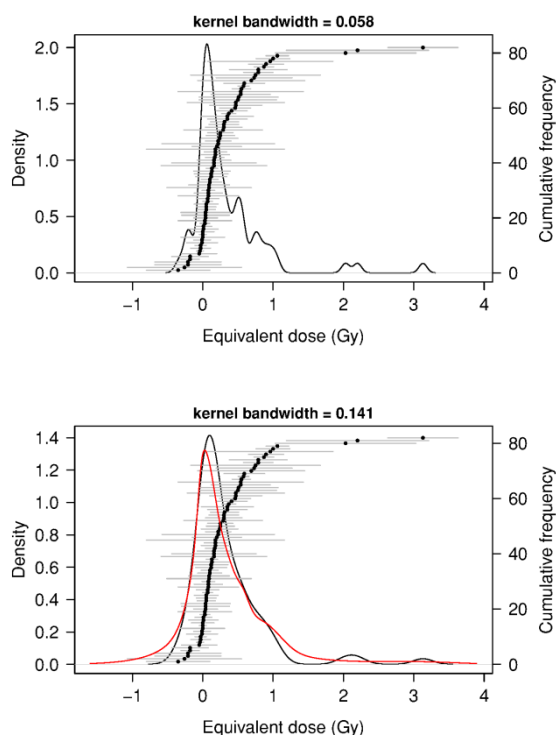
Figure 3: *Kernel density plots with two different bandwidths and empirical cumulative distributions for 82 single grain equivalent doses (data from Olley et al., 2004). The grey bars show ±1 standard error for each point. The red dotted curve shows a PD plot of these data.*

R function bw.nrd (one of several general rules of thumb). This is a larger bandwidth (0.141) giving a smoother graph. In some ways this version looks "nicer", but of course more resolution is lost. This is good if you think that such resolution is meaningless, but bad if it might be informative. Note that when plotting a KDE there is an implicit assumption that the data were sampled from a *continuous* distribution, and presumably one that is meaningful.

In the lower panel of Figure 3 I have added a PD curve (the red dotted line). The scale is chosen so that the area under it is the same as that for the KDE. Given that it does not represent the distribution of either the true or observed D_e values, what use is it? In this example, it is even smoother than the KDE in that panel and its mode is lower (practically zero). Perhaps its worst feature, though, is its behaviour in the lower tail. We know that the true doses cannot be negative, so a negative observed dose gives us a lower bound on the absolute size of the *actual* error for that grain. For example, if we observed a D_e of −0.2 Gy, then, because the true value for that grain cannot be negative, the estimation error must be

negative and not less than 0.2 Gy in absolute value — i.e. the observed value must be (more than) 0.2 Gy below the true value (regardless of what the standard error is). Yet the PD plot still puts more area below even the lowest negative D_e.

There is another distinction between a PD plot and a KDE (or histogram) that is worth repeating: for larger sample sizes one normally uses a smaller bandwidth for a KDE (or bin width for a histogram). But a PD plot does not get any better, in terms of resolution, as the number of grains increases. In general it gets worse because there are more low precision points to obscure the information. For example, the sample sizes in Berger's four examples are, respectively, 22, 63, 56 and 179. It could be argued that the PD plot of the last one, in his Figure 10, is too smooth and that a KDE with a smaller bandwidth would show the data better.

Error bars and confidence intervals
The standard error bars in Figure 3 can be regarded as simply displaying the size of the standard error of each estimate. But they could also be regarded as indicating confidence intervals for the true values. In that case they would be approximate 68% intervals rather than the more conventional 95%, or two-sigma, intervals.

While this may be of some use, it is extremely hard to compare several confidence intervals of differing lengths, both visually and logically. One may be tempted to infer "significant or not" differences from seeing whether intervals overlap, though of course that would not be correct. There is no easy way to interpret a number of univariate confidence intervals together; in principle, a multivariate confidence region is required.

A widely recognised disadvantage of confidence interval plots is that the least precise estimates have the longest intervals and tend to dominate the space on the graph. Sometimes they can be so dense that it is counter-productive to draw them all and it would be better to try to find another method of displaying precisions.

Very often the standard errors increase with dose, which makes it still harder to compare them. In such cases it may be clearer to plot doses (and intervals) on a log scale. Another aspect of this is that a symmetric interval on the log D_e scale will not transform to a symmetric interval on the D_e scale. That is, the symmetric approximate 95% interval $\log(y_i) \pm 2r_i$ for the true log dose corresponds to the non-symmetric interval $y_i \exp(\pm 2r_i)$ for the true dose, which may differ somewhat from the symmetric

interval $y_i \pm 2s_i$, where y_i denotes an observed D_e value and r_i and s_i are its relative and absolute standard error, respectively. If we really are regarding the error bars as confidence intervals, then some thought should perhaps be given to how they are best defined and displayed. For example, if the estimation errors were thought to be essentially multiplicative, then it would make more sense to construct symmetric confidence intervals on the log scale.

Weighted means and selected data
In his examples, Berger (2010a) suggested that instead of using a minimum age model, a sufficient estimate of the burial dose can sometimes more simply be obtained from a weighted average of the D_e values for a selected subset of grains; and he further suggested that sometimes using a weighted average of log(D_e) values is better. However, whatever form of average might be used, the crucial questions here are: (a) which subset of grains should be selected? and (b) what are the bias and variance of the resulting estimate?

With respect to (a), many possibilities spring to mind. Among the more sensible would be methods that tried to select the complete group of "youngest" grains whose observed D_e values were consistent having a common burial dose, taking into account estimation error and natural variation between true doses with the same burial history. Ideally, one hopes to select all of the fully bleached grains and no others, though this is usually not possible — see my earlier comments with respect to Figure 2. There will nearly always be partially bleached grains having observed D_e values consistent with those for well bleached grains.

Galbraith (2010) noted that there is no good rationale for choosing the grains whose D_e values are close to the mode of a PD plot (i.e. choosing them because of this) even though that may sometimes produce an estimate close to the correct value. It might be more reliable to choose them by looking at the radial plot, which would at least make it easier to account for their differing precisions. But however you choose them you are bound, except in rare cases, to either include some partly-bleached grains or exclude some well-bleached ones.

With respect to (b), Galbraith (2010) noted that selecting grains with the lowest doses and treating them as if they were properly representative of well-bleached grains leads to biased estimates, sometimes grossly biased. For example, you can imagine that if you tried to be conservative and selected *only* the grains with the very lowest observed D_e values then you are likely to omit some higher values from well-

bleached grains and end up with an under-estimate of the burial dose. Many of the lowest observed values will be low because their estimation errors are negative, so they will be lower than the corresponding true values. Hence, such a subset would be biased towards grains whose observed D_e values are lower than the true values.

Furthermore it is not correct to apply the usual standard error formula for an estimate obtained from a sub-sample that has been selected on the basis of the observed D_e values. This would not be an independent sample in its own right and allowance would need to be made for the effect of the selection. Calculation of a valid standard error is difficult for an objectively selected sample and impossible for a subjectively selected one.

Berger (2010a) rightly noted that such estimates are less reliable than those based on the more formal minimum age models. The latter treat the problem as one of extracting a specific component from a mixture. As such, they do not attempt to select a subset of grains at all, but rather they assign to each grain a probability of belonging to the well-bleached component.

On the subject of weighted averages and combining data generally, I recommend the encyclopedia entry by Cox (1982). This is a lucid and insightful article from a high authority.

A note on Sircombe and Hazelton (2004)
An interesting paper by Sircombe and Hazelton (2004), cited by Berger (2010a), adds some further theoretical insight to the question of estimating a frequency distribution from observations measured with error. It is concerned with detrital zircon ages obtained by U-Pb dating. It considers data y_i generated by the equation

$$y_i = x_i + e_i$$

where x_i is sampled from a distribution with pdf $f(x)$ and e_i is randomly drawn from a normal distribution with mean 0 and known standard deviation s_i. Like Galbraith (2010), it discusses how difficult it is to estimate $f(x)$. It then considers two samples of data and proposes a way of measuring the dis-similarity of their two different $f(x)$s without explicitly estimating either of them. Interested readers might like to look at its Figures 1 and 3. The former shows two different true $f(x)$s that have the same observed distribution (when errors are added to the x_is) and the latter shows how their method can nevertheless distinguish between them. Particularly illuminating is the way

the standard deviations s_i are used; this is very different from how they are used in a PD plot.

In addition, Figure 5 of that paper shows ten detrital zircon age distribution plots obtained by "summing individual Gaussian distributions" which, as far as I can see, are what we are calling PD plots. They are presented simply to show the ten samples together in a small space so that they can be plotted against measures of dis-similarity between pairs of their underlying $f(x)$s. No inferences about $f(x)$ are made from these plots — indeed the authors explicitly say they are displaying the estimation errors as well as the age variation. That figure is undoubtedly informative, mainly because the estimation errors are small (in some cases very small) compared with differences between the single grain ages. These PD plots are very different from those normally encountered with OSL D_e data. Nevertheless, the error variation, though mostly relatively small, is still confounded with the age variation.

Summary

Frequency distributions of OSL equivalent doses are hard to understand, even when D_e is measured accurately, because they will reflect sampling, experimental and observational effects in addition to the key features of scientific interest. Histograms and kernel density estimates of D_e values are hard to interpret.

The "alternate form of probability-distribution plot" proposed by Berger (2010a) does not represent a proper probability distribution because of an incorrect transformation from the log scale. If it were plotted on a log scale it would be a PD plot in the sense of Galbraith (2010) — but using $\log(D_e)$ values and relative standard errors, rather than D_e values and absolute standard errors, as is implied in the abstract of Berger (2010a). If it were correctly transformed to the linear D_e scale it would often not differ greatly from a PD plot directly constructed on that scale. Berger's interpretations of his TPD graphs are based on a misunderstanding of what he plotted and his conclusion that they can "reveal meaningful relative structure in D_e distributions" (Berger 2010a, p.19) is not justified.

Galbraith (1988) and Galbraith (2010) discussed PD plots in the context of fission track ages and OSL equivalent doses, respectively. Such plots do not have a sound statistical basis and they have often been mis-interpreted in the literature. Berger (2010a) noted that PD plots have been criticised but did not recognise the substantive criticisms in those papers. PD plots have sometimes been used as an aid to selecting subsets of grains from which a weighted mean dose is calculated. This is not a reliable practice for the reasons given above.

References

Arnold, L.J., Roberts, R.G., Galbraith, R.F., DeLong, S.B. (2009) A revised burial dose estimation procedure for optical dating of young and modern-age sediments. *Quaternary Geochronology* **4**, 306–325.

Berger, G.W. (2010a) An alternate form of probability distribution plot for D_e values. *Ancient TL* **28**, 11–21.

Berger, G.W. (2010b) Errata: An alternate form of probability distribution plot for D_e values. *Ancient TL* **28**, 81.

Cox, D.R. (1982) Combination of Data, In *Encyclopedia of Statistical Sciences* (Vol 2, pp 45–52), Eds S. Kotz and N.L. Johnson, New York, Wiley.

Galbraith, R.F. (1988) Graphical display of estimates having differing standard errors. *Technometrics* **30**, 271–281.

Galbraith, R.F. (1998) The trouble with probability density plots of fission track ages. *Radiation Measurements* **29**, 125–131.

Galbraith, R. (2010) On plotting OSL equivalent doses. *Ancient TL* **28**, 1–9.

Olley, J.M., Pietsch, T., Roberts, R.G. (2004) Optical dating of Holocene sediments from a variety of geomorphic settings using single grains of quartz. *Geomorphology* **60**, 337–358.

Sircombe, K.M., Hazelton, M.L. (2004) Comparison of detrital age distributions by kernel functional estimation. *Sedimentary Geology*, **171**, 91–111.

Response to Galbraith

G.W. Berger

Desert Research Institute, 2215 Raggio Parkway, Reno, NV 89512, USA.

Introduction

Rex Galbraith and I exchanged many e-mails in 2010 concerning my note on so-called TPD plots (Berger, 2010a). As a result I submitted an Erratum (Berger, 2010b) which I think clarifies Berger's note succinctly. That e-mail exchange, as does his recent Comment (Galbraith, 2011), draws out an essential 'philosophical' difference. Perhaps the best way to summarize this difference is to say that I am concerned with "empirical distributions" and how to use visual representations of single-grain paleodose (D_e) estimates as accessible guides to choices of usefully accurate calculations of 'mean' D_e values, whereas he is describing the same 'elephant' from a statistically idealistic viewpoint. Clues to this idealism are provided by the frequent use in Galbraith (2011) of ill-defined (with respect to single-grain D_e data) words such as: 'true', 'useful', 'less informative', 'more informative', 'less meaning', 'less convincing', 'resolved', 'actual', etc. In the context, these words misrepresent the pragmatic message of Berger (2010a, 2010b). While I appreciate his current note as an attempt to educate the reader on the theoretical nuances of the statistical handling of single-grain D_e distributions and their embedded uncertainty estimates, and calculations of weighted means, for some of the reasons outlines above, the Comment (Galbraith, 2011) compels some reply herein.

One of the outcomes of our e-mail exchange was my request that he provide to the community of OSL users a software or spreadsheet 'program' for the ready computation of KDE plots such as shown in Figure 3 of Galbraith (2011). Presumably such plots can be generated (with effort by a novice) from the R statistical package, but most of us don't use that package routinely (I employ it for Arnold's unlogged MAM code: Arnold and Roberts, 2009), if at all. Another request was for dissemination of a software package for generating reasonably high-resolution radial plots (e.g., pdf files, rather than clipboard copies) via a user-friendly interface (GUI) that handles both linear and log D_e scales. He has not supplied that to me. In this context, the Comment of Galbraith (2011) could have been more helpful. The radial-plot software available from John Olley has an excellent GUI but it does not permit use of linear D_e scales, and creates only clipboard images of the plots. The radial-plot software from Vermeesch (2009) does permit creating high-resolution plots (saved as pdf files) and use of linear scales, but lacks many desirable user-selectable options (e.g. choosing centers of ±2σ bands and band fills) that the Olley package offers.

In addition to these general comments, I have some comments to make on specific sections of Galbraith (2011), under his topic headings.

Introduction

Here he states that Berger (2010a) "does not recognize the more fundamental problems noted in Galbraith (1998) and Galbraith (2010)". This is incorrect and misrepresentative. Berger (2010a) did not attempt a fundamental discussion of the underlying principles expounded in these citations. How can that lacuna then demonstrate a lack of recognition?

Transforming a probability density function

The Erratum (Berger, 2010b) makes it clear that the areas under the peaks of the TPD plot cannot be used as indicators of relative probability, thus much of this section of Galbraith (2011) is redundant.

What is Berger's TPD plot?

There appears to be a logical inconsistency, in that (implied in Galbraith, 2011) it is permissible to adjust bin-widths to construct histograms of data points ('univariate estimates', if you will) lacking equal uncertainties, but it is not permissible to create a visual plot (TPD) free of such forced 'bandwidth' choices (unless once thinks the choice of a Gaussian is 'arbitrary'). It is misleading to state (Galbraith, 2011) that "the role of the relative standard errors of D_e" is "arbitrary". Also, what does Galbraith (2011) mean by "clear-cut interpretation" in the statement that the "TPD plot has no clear-cut interpretation"? Does he mean 'statistically idealistic', or 'empirically pragmatic'?

Log transformations (or not) in radial plots

This section is unnecessary because Berger (2010b) clarified that issue, concisely.

Why are radial plots more informative?

Berger (2010a) gave examples (and the literature has many more) where a radial plot is essential, but Galbraith (2011) repeatedly uses idealistic words such as "completely explained", or "more informative" to imply that other plots are useless. Also, the word "enough" in the phrase "or that two is enough" in paragraph 4 or 5 (depending on what is

counted as a paragraph) has a different meaning for a pragmatic geochronologist than for an idealistic statistician. In Figure 9a of Galbraith (1988) (which the reader should read) and Figure 2 of Berger (2010a), I continue to see that the PD plot illustrates the presence of two modes and that this (existence of two modes) is the most parsimonious view of that data distribution. Of course, in a real data set one can easily violate Occam's razor and conceive of many embedded components, but what would be the (geological) meaning of that? In the next paragraph, Galbraith (2011) makes remarks about overlapping data points that apply equally to a PD plot (if one plots the data points and uncertainties with this plot).

Empirical distributions and kernel density estimates
The word "incorrectly" is a statistical usage, whereas in dating practice, these nuances in Galbraith (2011) are likely to be largely of a secondary or tertiary concern, because one often is (or should be) comparing OSL age estimates with numerical or stratigraphic age estimates obtained from other methods. Again, it would have been more helpful if user-friendly code or standalone software were provided for generating such KDE plots (with all their subjectivity). The rest of this section seems to imply that with real data within single-grain D_e distributions (rather than with statistically idealistic data points) every bump and wiggle should be resolved or would be informative (informative of what?). In dating practice, as stated implicitly (if not explicitly) by Berger (2010a), many single-grain D_e data points obtained from non-eolian deposits have no geological meaning. Generally, if non-eolian (not uniformly bleached optically) samples are collected carefully (this topic is addressed below), only the lowest D_e values would have meaning (last daylight exposure), unless there are stratigraphic indicators that a specific multi-depositional history could be preserved, or in carbonate-bearing deposits, evidence of significant β micro-dosimetry. An example would be provided by buried soil horizons, in which case the lowest D_e values might not relate to the main depositional process or event.

In other words, in the Figure 3 of Galbraith (2011) and in many published examples of single-grain D_e distributions, it is not important to 'resolve' (whatever that word might mean to readers) minor clusters of D_e values above the lowest 'age' group. Of course, deviations caused by unrecognized or uncorrectable effects of β micro-dosimetry fold into interpretations in some cases. Further folded into the generation of 'under-estimates' of 'true' single-grain D_e values are the effects of careless sample collection when deposits are heterogeneous. For example, as stated (Berger, 2010a), the use of brute-force tube or pipe sampling may introduce (no one has investigated this effect, to my knowledge) 'too-young' grains (from the sediment face) into the interior of the sample. There are published examples (e.g. supporting online material of Jacobs et al., 2008) of single-grain D_e distributions where the authors are motivated (by stratigraphic or archaeological evidence) to employ a central-age or finite-mixture model and to dismiss widely discordant 'too-young' D_e data points that may be artifacts largely of the sample collection method.

Error bars and confidence intervals
It is not "extremely hard" for me (and presumably most practicing geochronologists) "to compare several confidence intervals of differing lengths, both visually and logically". Also, why is it "counter-productive" to draw confidence intervals? Counter-productive to what? ...to prediction of certain statistical parameters, or to age estimation from empirical data?

Weighted means and selected data
There are several points of disagreement, and I think that merely citing a few standard books (e.g. Bevington and Robinson, 1982; Moroney, 1965; Topping, 1962) on treatment of uncertainties would have sufficed. However, I fail to understand parts of the fourth paragraph. For example, in a geological sense, how can there be "some higher values from well-bleached grains" (apart from Gaussian or other probability effects) if these values indeed have been well-bleached and share the same β micro-dosimetry, unless one considers such and other physical effects, which Galbraith (2011) does not mention? Also, negative D_e values more than one (estimated) standard deviation below zero are possible if one accepts Gaussian probability in the measurement of D_e values close to (and above) zero. Much of that paragraph's argument is hypothetical conjecture: statistical idealism disconnected from empirical settings.

Summary
I disagree with the final sentence in Galbraith (2011): "This" selection of subsets of data points "is not a reliable practice...". Galbraith's definition of 'reliable' apparently is not mine. There are several examples in the single-grain OSL dating literature where selection of subsets provides usefully accurate (geologically, stratigraphically) age estimates. Of course, there are several examples in such literature where selection of subsets by use of visualization plots is too subjective (see some examples in Berger, 2010a) to be useful, and one must resort to more refined statistical calculation schemes (e.g., minimum-age, central-age models, Galbraith et al., 1999) than use of weighted means.

References

Arnold, L. J., Roberts, R. G. (2009) Stochastic modeling of multigrain equivalent dose (D_e) distributions: Implications for OSL dating of sediment mixtures. *Quaternary Geochronology* **4**, 204-230.

Berger, G.W. (2010a) An alternate form of probability distribution plot for D_e values. *Ancient TL* **28**, 11-21.

Berger, G.W. (2010b) Errata: An alternate form of probability distribution plot for D_e values. *Ancient TL* **28**, 81.

Bevington, P.R., Robinson, D.K. (2003) *Data Reduction and Error Analysis for the Physical Sciences*. McGraw Hill, New York.

Galbraith, R.F. (1988) Graphical display of estimates having differing standard errors. *Technometrics* **30**, 271-281.

Galbraith, R. (2010) On plotting OSL equivalent doses. *Ancient TL* **28**, 1-9.

Galbraith, R. (2011) Some comments arising from Berger (2010). *Ancient TL* **29**, 41-47.

Galbraith, R.F., Roberts, R.G., Laslett, G.M., Yoshida, H., Olley, J.M. (1999) Optical dating of single and multiple grains of quartz from Jinmium rock shelter, northern Australia: part I, experimental design and statistical models. *Archaeometry* **41**, 339-364.

Jacobs, Z., Roberts, R. G., Galbraith, R. F., Deacon, H. J., Grün, R., Mackay, A. W., Mitchell, P., Vogelsang, R., Wadley, L. (2008) Ages for the Middle Stone Age of Southern Africa: Implications for human behavior and dispersal. *Science* **322**, 733-735.

Moroney, M.J. (1965) *Facts from Figures*. Penguin Books, London, UK.

Topping, J. (1962) *Errors of Observation and their Treatment*. Chapman and Hall, London, UK.

Vermeesch, P. (2009) Radial Plotter: A Java application for fission track, luminescence and other radial plots. *Radiation Measurements* **44**, 409-410.

Message from the Editor

Following the long discourse that has ensued in the last two issues of Ancient TL, the Editorial Board has decided to clarify the maximum length of Letters and Replies. The purpose of this is not to stifle discussion, but rather to ensure that readers are able to clearly follow the line of argument arising from the original article. In the future, Letters to Ancient TL will be limited to a maximum of two printed pages, including diagrams, tables and references (equivalent to about 1400 words of text). Replies will have the same limit.

G.A.T. Duller

Errata: Estimating the error in equivalent dose values obtained from SAR

G. W. Berger

Desert Research Institute, 2215 Raggio Parkway, Reno, NV 89512, USA
(e-mail: glenn.berger@dri.edu)

_____

Errata

In the paper by Berger (2010) there are some typographical/transcription errors in some of the equations, all but one error relating to the saturating-exponential (E) model. Only one of these errors (that in the matrix component I_{aa} concerning the E model) occurred also in the author's software and led to some incorrect error estimates for some of the D_E values derived from the E-model data sets, but had no effect on the computed D_E values and on the best-fit dose-response curves (DRC) for the E model.

In equation 12 of Berger (2010),

$$\Delta A = ([WU]^t[WU])^{-1}([WU]^t[WY^*])$$

for the iterative calculation of the best-fit parameters, the matrix W should be replaced by $\sqrt{W}$. In the immediately subsequent equation for wy*, brackets were inadvertently omitted during transcription. The correct equation is

$$wy^* = [y_i - a(1 - e^{-bx_i})]\sqrt{w_i}$$

In the subsequent subsection "5.2 Error in D_E", the equations for the matrix components I_{aa}, I_{bb} and I_{ab} are incorrect. Certain parameters were inadvertently omitted during transcription. The correct expressions are as follows:

$$I_{aa} = \sum_i w_i(1 - e^{-bx_i})^2$$
$$I_{bb} = \sum_i w_i(ax_i e^{-bx_i})^2$$
$$I_{ab} = I_{ba} = \sum_i w_i f_i x_i e^{-bx_i}$$

Finally, at the end of the first paragraph in the subsection "6.1 Regression to obtain a, b, c" for the E+L model, the stated matrices *WU* and *WY** should be replaced by $\sqrt{W}U$ and $\sqrt{W}Y^*$.

The consequence of the coding error in the equation for I_{aa} (used in the calculation of errors in the D_E values shown in the paper) is as follows. In Table 1, the last two D_E values in the last column should read 0.698 ± 0.062 (not ± 0.058), and 28.48 ± 0.69 (not ± 0.68). In Table 3, the only changes (all in the last column) are: 2104 ± 255 (not ± 128), and 1417 ± 668 (not ± 148). These changes put the author's error estimates (for the E model) in Table 3 closer to those from Duller's (2007) 'curve-fitting' error estimates, and strengthen one of Berger's (2010) conclusions: that the two error-estimation schemes (Berger's and Duller's) generally produce no significantly different error estimates.

References

Berger, G.W. (2010) Estimating the error in equivalent dose values obtained from SAR. *Ancient TL* **28**, 55-66.

Duller, G.A.T. (2007) Assessing the error on equivalent dose estimates derived from single aliquot regenerative dose measurements. *Ancient TL* **25**, 15-24.

Submission of articles to Ancient TL

Reviewing System

In order to ensure acceptable standards and minimize delay in publication, a modification of the conventional refereeing system has been devised for Ancient TL:

Articles can be sent directly by authors to a member of the Reviewers Panel chosen on the basis of the subject matter, but who is not in any of the authors' laboratories. **At the discretion of the Editor**, reviewers who are not listed in the Panel may be used.

The reviewing system aims to encourage direct dialogue between author and reviewer. The Editor should be kept advised of the progress of articles under review by sending him copies of all correspondence. He is available for advice where reviewing difficulties have arisen. Authors whose mother tongue is not English are required to have their manuscript revised for English *before* submitting it.

We ask reviewers to specify (where required) the minimum of revision that is consistent with achieving a clear explanation of the subject of the paper, the emphasis being on *rapid* publication; reviewers are encouraged to make a brief written comment for publication at the end of the paper. Where a contribution is judged not to meet an adequate standard without substantial modification, the author will be advised that the contribution is not suitable for publication. Articles that are not considered to be of sufficient interest may also be rejected.

Procedures

1. Articles should be submitted to an appropriate member of the Reviewing Panel or Editorial Board, chosen on the basis of the subject matter, but who is not in any of the authors' laboratories.
2. Articles should not normally exceed the equivalent of 5000 words inclusive of diagrams, tables and references. Greater space will be appropriate for certain topics; for these the Editor should first be consulted.
   Short notes and letters are also invited. These should not exceed two printed pages in Ancient TL, including diagrams, tables and references (equivalent to ~1400 words of text).
3. Diagrams and labels should be ready for direct reproduction and not normally exceed 12 cm wide by 10 cm high. Where possible, high quality electronic versions of figures should be submitted. Separate figure captions should be supplied. Inappropriately scaled drawings and labels will be returned for alteration.
4. Authors are asked to submit the paper, including diagrams, to the Reviewer and a duplicate copy to the Editor.
   The final version of the text must be submitted to the Editor electronically using a standard format (Microsoft Word for PC is currently used for producing Ancient TL). Electronic copies of Diagrams and Tables should also be submitted.
5. Upon receipt of an article, the Editor will send an acknowledgement to the author. If the Reviewer is unable to deal with the contribution within **4 weeks** he/she will inform the author and advise the Editor.

Requirements under various situations

When agreement concerning an article has been reached:
The Editor should receive a copy of the final version of the paper, both as hard copy and electronically. The Reviewer should send their final decision, including comments for publication if any, to the Editor.

If the article has not been rejected, but agreement on its final form cannot be reached or where there are protracted delays in the reviewing process:
The Editor may request an assessment from the Reviewer and responsibility passes to the Editor.

If the article is rejected:
The Editor and author receive notification from the Reviewer, with an indication of the reason for rejection.

Thesis abstracts are to be sent to the Editor and in principle do not need reviewing. However, authors are requested to make sure that the English is correct before submission. Thesis abstracts should not exceed 750 words, and figures and tables are not accepted.

Advertising. Formal information on equipment can be published in Ancient TL. It should not exceed one printed page. Current charges are displayed on the website (http://www.aber.ac.uk/ancient-tl)

Subscriptions to Ancient TL

Ancient TL is published 2 times a year and is sent Airmail to subscribers outside the United Kingdom. While every attempt will be made to keep to publication schedule, the Editorial Board may need to alter the number and frequency of issues, depending on the number of available articles which have been accepted by reviewers.

The subscription rate for 2011 is £15 for individual subscribers and £25 for Institutional subscription, plus any taxes where required. Payment must be in pounds sterling. Enquiries and orders must be sent to the Editor. Payment may be by cheques, made payable to 'Aberystwyth University', by credit/debit cards or by bank transfers. Further information on subscriptions is available on the Ancient TL web site (**http://www.aber.ac.uk/ancient-tl**)